The nonlocal impacts of Antarctic subglacial runoff

Daniel N Goldberg[1], Andrew G Twelves[1], Paul Richard Holland[2], and Martin Graeme Wearing[1]

[1]University of Edinburgh
[2]British Antarctic Survey

March 13, 2023

Abstract

Little is known about Antarctic subglacial hydrology, but based on modeling, theory and indirect observations it is thought that subglacial runoff enhances submarine melt locally through buoyancy effects. However, no studies to date have examined effects of runoff on sea ice and circulation on the continental shelf. Here we use modeled and observational estimates of runoff to force a regional model of the Amundsen Sea Embayment. We find that runoff enhances melt locally (i.e. within the ice-shelf cavity), increasing melt at Thwaites ice shelf by up to 15 Gt/a given estimates of steady runoff, and up to 25 Gt/a if runoff is episodic as remote sensing measurements suggest. However runoff also has smaller nonlocal effects through freshwater influence on flow and stratification. We further find that runoff reduces summer sea-ice volume over the continental shelf (by up to 10\% with steady runoff but over 30\% with episodic runoff). Furthermore runoff is much more effective at reducing sea ice than an equivalent volume of ice-shelf meltwater – due in part to the latent heat loss associated with submarine melting. Results suggest that runoff may play an important role in continental shelf dynamics, despite runoff flux being small relative to ice-shelf melting – and that runoff-driven melt and circulation may be an important process missing from regional Antarctic ocean models.

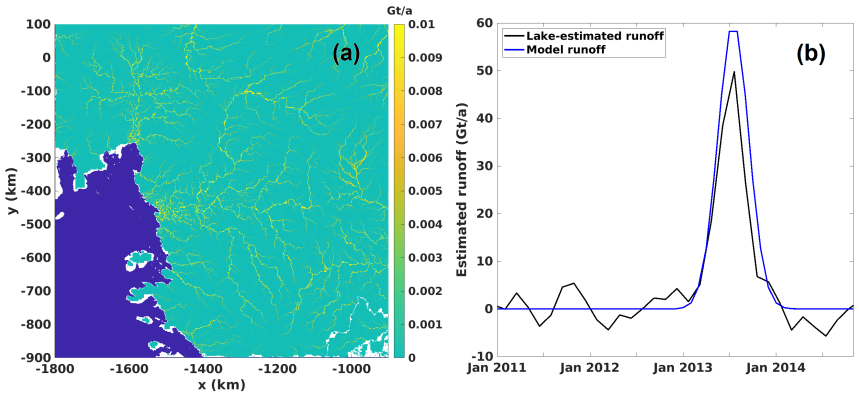

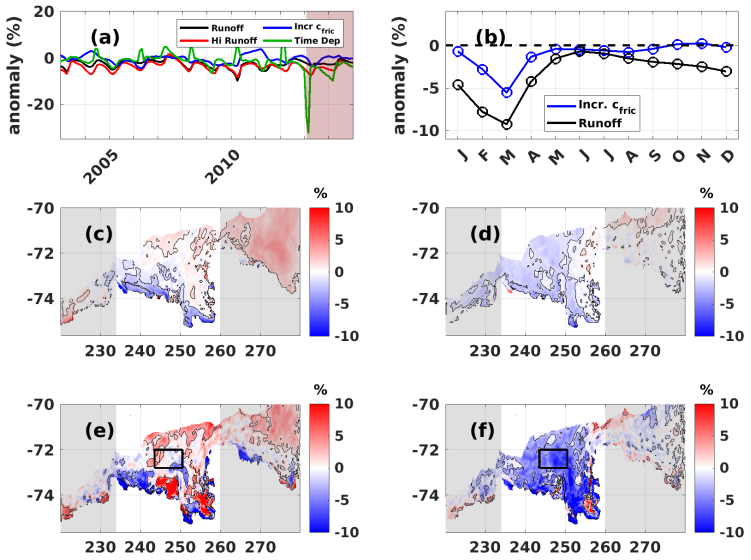

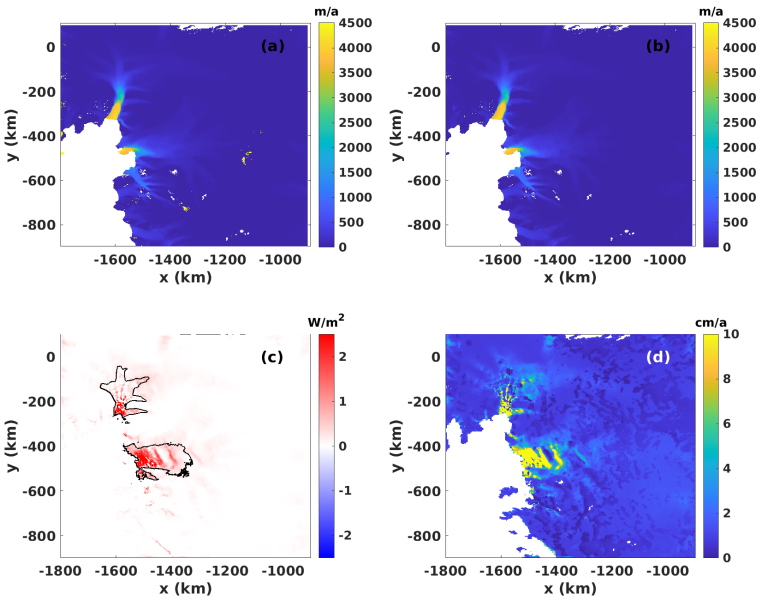

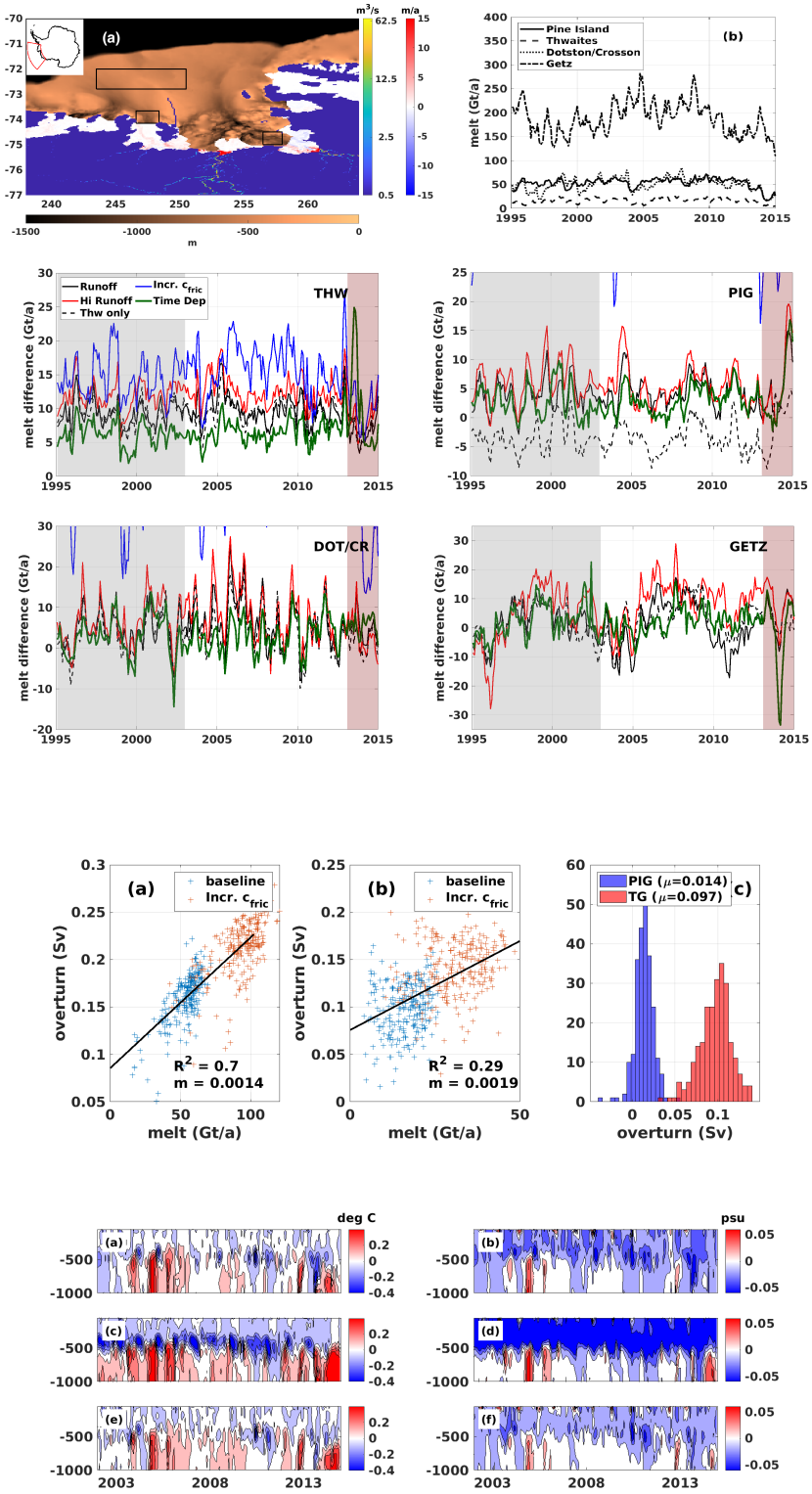

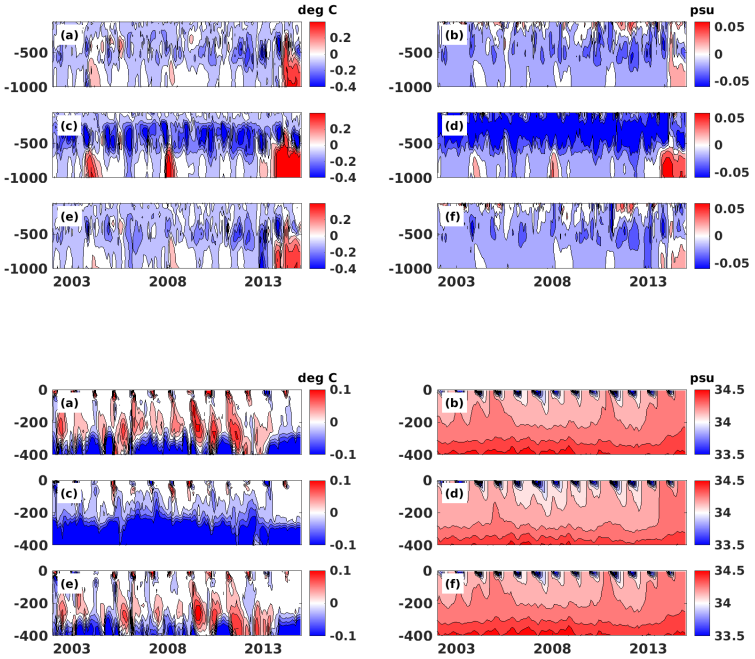

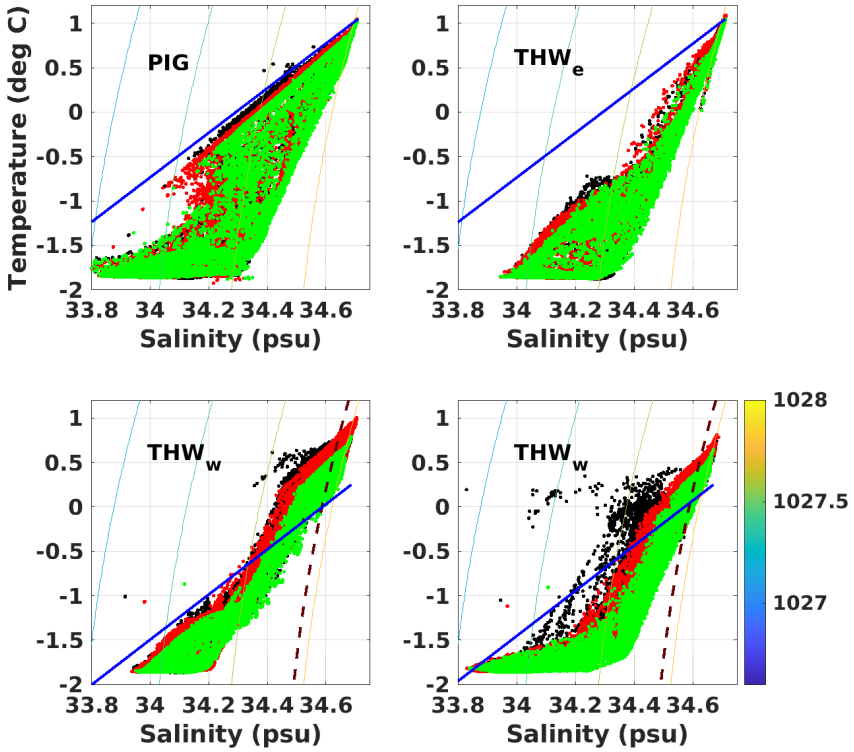

The nonlocal impacts of Antarctic subglacial runoff

Daniel N Goldberg[1], **Andrew G Twelves**[1], **Paul R Holland**[2], **Martin G Wearing**[1]

[1]School of GeoSciences, University of Edinburgh, Edinburgh, UK
[2]British Antarctic Survey, Cambridge, United Kingdom

Key Points:

- modeled and observational runoff estimates are used to force a regional model of the Amundsen Sea Embayment
- Runoff has a strong local effect on ice-shelf melting but can influence ice-shelf melt nonlocally as well
- Runoff impacts on sea ice differ qualitatively from those of an equivalent volume of ice-shelf melting

Corresponding author: Daniel N Goldberg, dan.goldberg@ed.ac.uk

Abstract

Little is known about Antarctic subglacial hydrology, but based on modeling, theory and indirect observations it is thought that subglacial runoff enhances submarine melt locally through buoyancy effects. However, no studies to date have examined effects of runoff on sea ice and circulation on the continental shelf. Here we use modeled and observational estimates of runoff to force a regional model of the Amundsen Sea Embayment. We find that runoff enhances melt locally (i.e. within the ice-shelf cavity), increasing melt at Thwaites ice shelf by up to 15 Gt/a given estimates of steady runoff, and up to 25 Gt/a if runoff is episodic as remote sensing measurements suggest. However runoff also has smaller nonlocal effects through freshwater influence on flow and stratification. We further find that runoff reduces summer sea-ice volume over the continental shelf (by up to 10% with steady runoff but over 30% with episodic runoff). Furthermore runoff is much more effective at reducing sea ice than an equivalent volume of ice-shelf meltwater – due in part to the latent heat loss associated with submarine melting. Results suggest that runoff may play an important role in continental shelf dynamics, despite runoff flux being small relative to ice-shelf melting – and that runoff-driven melt and circulation may be an important process missing from regional Antarctic ocean models.

Plain Language Summary

A number of floating ice shelves in Antarctica are exposed to warm waters which lead to strong melting, limiting shelves' ability to buttress against ice flow from the continent and also bringing warmed and freshnened waters to the ocean surface – waters which in turn influence seasonal sea ice near the continent and insulate the deep ocean from the cold atmosphere. Meanwhile, large rivers under the Antarctic ice sheet carry melt from the ice sheet base to the ocean cavities beneath ice shelves. While a few studies have looked at the role these rivers play in ice-shelf melt, none have examined these effects in a regional context. We find that these "rivers" not only amplify melting under ice shelves, but have far-reaching impacts on ocean circulation. We find that while the direct contribution of water from these subglacial rivers is small compared to that of ice-shelf melt, there is a disproportionate impact on seasonal sea ice.

1 Introduction

The ice shelves of the Amundsen Sea Embayment contribute several hundred gigatonnes of melt water per year to the ocean (Adusumilli et al., 2020). In addition to causing a loss of buttressing that can lead to sea level rise (Favier et al., 2014; Joughin et al., 2014; Seroussi et al., 2017; Goldberg & Holland, 2022), the flux of fresh water has impacts on the ocean as well. Ice-shelf melt drives upwelling of large volumes of Circumpolar Deep Water (CDW) and thinning of sea ice on the continental shelf (Jourdain et al., 2017) – the latter of which could have implications for biological production in seasonal polynyas (Arrigo et al., 2012). The addition of freshwater can stratify the ocean and also feed back on delivery of CDW to ice-shelf cavities (Kimura et al., 2017; Mathiot et al., 2017; Silvano et al., 2018; Bett et al., 2020).

Subglacial discharge at ice-shelf grounding lines is another source of fresh water. Like ice-shelf melt, it adds buoyancy at depth, which leads to upwelling of dense waters. At tidewater glaciers in Greenland and elsewhere, it is known that subglacial runoff leads to upwelling and strong melt at the terminus (e.g., Jenkins, 2011; Motyka et al., 2013; Slater et al., 2015), but also influences circulation within the fjord (Cowton et al., 2016; Slater et al., 2018). In Antarctica, subglacial runoff is observed to induce strong grounding-line melt and ice-shelf channel formation (Le Brocq et al., 2013; Drews et al., 2017), but few studies have attempted to quantify its impact on ocean physics. This is partially because comparatively little is known about Antarctic subglacial hydrology: little supraglacial melt is transported to the bed, melt is generated through frictional heating and geother-

mal flux (Van Liefferinge & Pattyn, 2013), and runoff is very poorly constrained. Still, Joughin et al. (2009) calculated subglacial melt values of 1.7 and 3.5 Gt/a for the catchments of Pine Island and Thwaites glaciers, respectively, similar to annual runoff for large Greenland glaciers (Mernild, Howat, et al., 2010; Mernild, Liston, et al., 2010). These mean values are small relative to ice-shelf melt, but observations of subglacial lake drainage suggest rates up to 50 Gt/a or more could be sustained for months (Smith et al., 2017; Malczyk et al., 2020). It is therefore reasonable to ask how this runoff impacts submarine melt and ocean circulation, and how this varies with runoff magnitude and temporal character.

Nakayama et al. (2021) used a high-resolution model of Pine Island ice shelf cavity with a representation of runoff, in order to explain high satellite-observed melt rates which are not captured by models considering CDW alone. That study considered steady states only, and did not examine impacts on continental shelf circulation. In this paper we apply modeled runoff from the catchments of Pine Island, Thwaites, Smith, and Getz glaciers to a regional sea ice-ocean-ice shelf model of the Amundsen Sea. The model is run for two decades; both time-constant and varying runoff scenarios are investigated in terms of impacts on ice-shelf melt, sea-ice coverage, and ocean conditions on the continental shelf.

2 Methods

2.1 Regional ocean model

We model regional sea ice, ocean circulation and ice-shelf melt with the MITgcm (Marshall et al., 1997; Losch, 2008; Losch et al., 2010). The configuration is very similar to that of Naughten et al. (2022), which builds upon that of Kimura et al. (2017) and Bett et al. (2020). The domain extends from 220-290° longitude (i.e. 140 to 70°W) and 75.65-62.4°S, with resolution approximately .025° latitude (∼2.5 km) on the Amundsen shelf. Bathymetry and ice-shelf draft are interpolated from BedMachine Antarctica version 2 (Morlighem et al., 2020). Ocean-facing boundary conditions are sourced from the World Oceanographic Atlas (Zweng et al., 2019; Locarnini et al., 2018) and the B-SOSE state estimate (Verdy & Mazloff, 2017), and surface forcing is from ERA5. The Bear Ridge iceberg "wall" and iceberg freshwater flux from Bett et al. (2020) is used. Our model differs from that of Naughten et al. (2022) only in that rather than the Merino et al. (2016) iceberg freshwater flux, that of our model assumes a constant flux along the coastline. The impacts of this choice of iceberg flux were found to be negligible (K Naughten, pers. comm.), and so in this study we consider results of our **baseline** experiment (see below) to reflect those of Naughten et al. (2022).

Naughten et al. (2022) provides validation against available oceanographic and remotely-sensed observations. Thermocline depth at Pine Island is captured well, but less so in front of Dotson Ice Shelf. Deep temperatures for both are underestimated post-2012 but well captured before. Temporal evolution and maximum extent of sea ice is well captured though summer extent is somewhat underestimated. Inter-annual melt variability is well captured for Dotson and Pine Island, but Pine Island melt magnitude is slightly underestimated, especially in the late 2000s. Thwaites melt is low relative to Adusumilli et al. (2020), though there are no oceanographic estimates yet available to compare. Importantly, the tuning of this configuration did not take subglacial runoff into account. We refer below to this configuration as the **baseline**. For more detail on the configuration see Naughten et al. (2022).

2.2 Subglacial runoff

In most of our experiments, our ocean model is forced with subglacial runoff. Our calculation of runoff volumes and locations is described here, followed by description of how runoff is implemented in the ocean model.

Melt calculation

In order to provide an estimate of time-mean runoff at the grounding line, we first estimate the pattern of subglacial melt. To do so we solve the basal heat balance (e.g., Joughin et al., 2009; Cuffey & Paterson, 2010):

$$m_b = \frac{G + \tau_b u_b - k_i \Theta_i}{L_i \rho_i}, \tag{1}$$

where m_b is basal melt rate, G is geothermal flux, k_i is thermal conductivity, Θ_i is ice basal temperature gradient, L_i is ice latent heat, ρ_i is ice density, and τ_b and u_b are basal drag and speed, respectively.

To calculate the frictional heating term $\tau_b u_b$, we use the ice-sheet model STREAMICE (Goldberg & Heimbach, 2013), which uses a higher-order approximation to Stokes flow and is capable of representing vertical shear as well as fast sliding flow regimes. To estimate $\tau_b u_b$ an inversion is carried out for basal drag and ice stiffness parameters. As described in Goldberg and Holland (2022), the stiffness parameter is initialised using a modeled temperature distribution (see below), and is allowed to vary though deviation from this initial distribution is penalised within grounded portions of the domain. The ice-sheet model is run at 2 km resolution over the Amundsen region (Fig. 1), and the MEaSUREs (Rignot et al., 2011) Version 2 product, interpolated to the domain, constrains the inversion (Fig. 1a,b). The resulting basal velocity and basal drag are then used to generate the frictional heating term. Ice-sheet inversion requires specification of regularisation parameters to prevent ill-posedness (Goldberg et al., 2019). The influence of these parameters on the model-observation fit was investigated, but they were found to have little impact on large-scale melt rates.

Heat flux from Martos et al. (2017) is used for G, with a topographic correction to account for small spatial scales Colgan et al. (2021). STREAMICE does not have a thermomechanical component, therefore a modeled estimate of ice temperature (Van Liefferinge & Pattyn, 2013) is used to calculate the vertical gradient, as well as for generation of the initial guess for ice stiffness. The vertical conduction term (Supplemental Fig. S1(a)) is small relative to the geothermal heat flux and frictional heating: the domain-integrated contribution of conduction is approximately 2×10^{11} W, which is approximately 10% of either dissipation or geothermal flux. Since geothermal flux (Supplemental Fig. S1(b)) and dissipation are uniformly nonnegative and conduction is uniformly nonpositive, conduction accounts for approximately 10% of melt – meaning that even large errors in this term will have a small effect on overall melt and runoff at the grounding line.

In a sensitivity experiment, the components of the above calculation are modified as follows: G and Θ_b remain the same, but frictional dissipation $\tau_b u_b$ is increased within the regions of fast flow of Pine Island and Thwaites (Fig. 1(c)). Within each of the regions indicated, dissipation is increased uniformly by an amount equal to the mean frictional heating within that region. The rationale behind this experiment is that if there is a change in melt volume in the future, it will likely be due to a change in frictional effects rather than in geothermal flux. However, the imposed change in frictional heating is not based on ice-sheet projections, it is simply a means of assessing the impact of larger runoff.

Subglacial routing

We use the routing model of Le Brocq et al. (2009) to determine the flux at the grounding line. Le Brocq et al. (2009) uses a laminar flow closure which relates subglacial flow velocity to background hydraulic potential, and uses this to derive a steady-state solution for subglacial flux. Subglacial flow is not coupled to water pressure in the model, and so model hydraulic potential depends only on ice thickness and bed elevation. The BedMachine Antarctica version 2 product (Morlighem et al., 2020) is used for these fields. Fig. 2(a) shows the routing solution using the melt from Fig. 1(d).

Time dependent runoff

The above calculations generate a time-independent melt rate, intended to represent the average melt over long time periods. However, lake-drainage observations suggest that runoff is strongly time-varying. For time-dependent runoff, the time series of (Malczyk et al., 2020) is considered. The data describes volume change rates of 4 active lakes in the upstream part of Thwaites glacier. A time series of total volume loss is found by summing the contributions of all lakes. The result (Fig. 2(b)) shows intra-annual variability on the order of 3-5 Gt/a over the 2011-2015 period, but the most noticeable feature is a pulse of up to 50 Gt/a that lasts for about 1 year (2013-2014).

In the experiment forced by time-dependent runoff, an assumption is made that the water which collects in these lakes is mainly drainage from the upstream, slower-flowing parts of the catchment where there is relatively little frictionally-driven heating. Thus, we partition runoff into a steady component, driven by frictional heating and thermal conduction alone; and a time-dependent component. The steady component is found simply by setting geothermal heat flux to zero and routing the melt as described above. For the time-dependent component, the runoff flux is set to zero for all cells away from the Thwaites grounding line, and flux along the grounding line is scaled so that the total flux (for the time-dependent component) follows the idealised time series in Fig. 2(b). In other words, there is a steady runoff along the grounding line of the domain corresponding to frictional heating only, and from 2013-2014 there is an additional pulse representing lake drainage.

Our experimental design implicitly assumes a one-to-one correspondence between lake drainage and runoff, which is unlikely due to transit time, subglacial storage, and the potential for unobserved lakes or drainage out of the Thwaites catchment. It also neglects additional subglacial melt due to frictional heating associated with channelised flow. Its simplicity reflects the fact that very little is still known about the Antarctic subglacial environment. Still, our representation captures to leading order the evidence that there is episodic drainage from upstream portions of Thwaites, but that areas closer to the grounding line exhibit efficient drainage (Schroeder et al., 2013; Hager et al., 2022). As our aim is to examine the impacts of episodic runoff, it is likely appropriate.

2.3 Implementation of runoff in ocean model

In order to implement runoff within MITgcm, the grounding line runoff from the routing product described above is first interpolated to the ocean grid. The grid of the routing model is in polar-stereo coordinates with 500 m resolution, and the ocean grid is in latitude/longitude coordinates with an approximately 2.5 km resolution, so the grounding line of the ocean model does not perfectly align with the edge of the routing domain. Runoff is therefore interpolated as follows. The output of the routing model is a gridded field which contains volumetric fluxes (in m^3/s) that represent the flux coming out of each cell. Cells where the routing network terminates are identified. For each one of these cells, the flux is allocated to the nearest nonempty ocean column, generating a 2D field which is used to force the ocean model.

The runoff is assumed to enter the ocean with zero salinity and to be at the pressure-depressed freezing point. At each time step of the ocean model, in columns with nonzero grounding line flux as determined by the process above, the salt and temperature tendency in the deepest ocean cell are thus updated according to this flux value:

$$\frac{dS_{i,k}}{dt} = \frac{Q_i(0 - S_{i,k})}{A_i h_k}, \tag{2}$$

$$\frac{dT_{i,k}}{dt} = \frac{Q_i(p_{i,k}b - T_{i,k})}{A_i h_k}, \tag{3}$$

where i refers to the column, and k to the depth level, of the bottom cell; $S_{i,k}$, $T_{i,k}$, and $p_{i,k}$ are the salinity, temperature, and pressure, respectively, of the cell at the current time step; Q_i is the flux into the column; and b is the freezing point dependence on pressure (set to -7.61$\times 10^{-4}$ °C per dbar). Where the bottom cell is below a minimum thickness (in this study 40 m), the tendency is distributed over the bottom two cells in a conservative fashion similar to the under-ice shelf boundary layer treatment of (Losch, 2008), in order to prevent overly strong freshening and cooling. The above changes are made to MITgcm version 67v.

The treatment does not affect ocean momentum (velocities) – this is in contrast to Nakayama et al. (2021) and Slater et al. (2015), which implement runoff through open boundary conditions. However, given the low resolution of the model, this impact is likely to be small. Consider a channelised flux of magnitude Q entering an ocean cell with an associated volume V through an opening of area A. There is therefore an associated momentum flux of $\rho Q u$ into the ocean cell, where u is the speed of the runoff. The associated rate of change of velocity within the cell can be estimated as

$$\begin{aligned}\frac{du}{dt} &= \frac{uQ}{V} \\ &= \frac{Q^2}{VA}.\end{aligned} \tag{4}$$

With a runoff flux of 300 m^3/s $\approx$ 10 Gt/a, a channel with a half-circular geometry and radius of $\sim$10 m, and a cell volume of 2.5 km $\times$ 2.5 km $\times$ 40 m, this leads to an acceleration of $\sim$ 0.0025 mm/s^2, or a change of $\sim$ 1.5 mm/s over a 600 second time step. Moreover, results from buoyant plume theory (e.g., Slater et al., 2016) suggest that a buoyant plume driven by subglacial discharge quickly adjusts to a state which is insensitive to initial conditions.

2.4 Ice-shelf cavity overturning

In the analysis of sea-ice response to runoff, rates of volumetric overturning under the Amundsen ice shelves are calculated. In this calculation the horizontal convergence of flow below a certain depth is taken as a proxy for overturning. Convergence is calculated by integrating horizontal convergence of velocity at each depth layer underneath the ice shelf, giving the net flux per unit depth leaving the cavity at that depth level. This quantity is then integrated vertically up to a certain depth, chosen as the depth for each ice shelf below which there is predominantly inflow of warm water. This depth is chosen as 600 m for Thwaites and 550 m for Pine Island (Supplemental Fig. S2).

2.5 Experiments

We refer to the ocean simulations forced by the two steady runoff cases as the **runoff** and **hi runoff** experiments, and to the run forced by lakes data as **time dependent runoff**. Additionally, we consider a scenario without runoff but where c_{fric}, the drag coefficient governing ice shelf basal melting (Dansereau et al., 2014), is increased (from 0.004 to 0.01) – the purpose being to assess the sensitivity to freshwater sourced from

ice shelf melting as opposed to subglacial runoff. Specifically, the value of c_{fric} is chosen so that the time-mean melt increase for Thwaites ice shelf (relative to **baseline**) is similar to the increase in fresh water discharge (combined runoff and melt) from Thwaites in the **runoff** experiment. This basis of comparison is chosen due to our focus on Thwaites in the Discussion (Section 4). This experiment is referred to as the **increased c_{fric}** experiment. Finally, an experiment (**Thwaites only**) is carried out where runoff is as in the **runoff** experiment, but set to zero away from the Thwaites grounding line. Each experiment is run for 20 years from 1 Jan 1995 to 31 Dec 2014, beginning from the saved state of the baseline run. A freshwater tracer for combined runoff and ice-shelf melt is implemented in the **baseline** experiment.

In the **runoff** experiment, the majority of the runoff enters the Amundsen through three large channels beneath Thwaites and Pine Island glaciers (Fig 3). The total runoff across the Thwaites and Pine Island grounding lines are approximately 4.6 and 2.7 Gt/a, respectively. These values are larger than those cited in Joughin et al. (2009), though this could result from the use of a different GHF estimate (Joughin et al. (2009) used a constant value for GHF), a more recent velocity estimate, or both. In **hi runoff** these increase to 6.8 and 3.9 Gt/a, respectively. Meanwhile, at most 0.4 Gt/a enters from each of the Dotson/Crosson and Getz grounding lines. In **time dependent runoff**, runoff reaches nearly 50 Gt/a, but only for a few months (Fig. 2(b)).

We emphasize that neither the **runoff**, **hi runoff** nor the **time dependent runoff** forcings are intended as the "correct" representation of subglacial runoff in a spatial or temporal sense. Rather, we present our scenarios as end-members representing time-constant and episodic modes of runoff. Furthermore, the ocean model used is too coarse to capture detailed melt patterns of ice-shelf melt response to runoff, which is better represented by high-resolution studies (Nakayama et al., 2021). Our focus is rather on impacts on total (ice-shelf wide) melt, as well as changes in sea ice and shelf hydrography, which the model is capable of capturing.

Examination of the freshwater tracer in the **baseline** experiment shows a domain-mean concentration that rises steadily to $\sim 6‰$ from 1995 to 2003, after which it varies by less than 10% (Supplemental Fig. S3). From this it inferred that the adjustment time of the system to the input of a tracer (such as freshwater runoff) is approximately 8 years. Therefore any "nonlocal" effects of runoff on melt may not be fully realised until after this time, whereas the response of melt to "local" runoff is much faster (Nakayama et al., 2021). Therefore, in our study "local" impacts of runoff on ice-shelf melt and overturning are analysed for the full 1995-2015 period, whereas "nonlocal" effects on ice-shelf melt, and sea-ice and ocean characteristics on the continental shelf, are analysed over the 2003-2015 period. (In the **time dependent runoff** experiment, which is inherently transient, there is no assumption of adjustment to the episodic runoff.)

3 Results

3.1 Ice-shelf melt

We center our discussion around the high-melting ice shelves in the Amundsen Sea, namely Pine Island, Thwaites, Dotson and Crosson (or Dotson/Crosson), and Getz. Fig. 3(a) shows the additional melt under these shelves in the **runoff** experiment, relative to **baseline**, averaged over the 20-year run. The strongest melt impacts are close to subglacial inputs (as seen from comparison with routing results) but there are also more distal effects under Pine Island and Dotson/Crosson. Melt time series from **baseline** are shown in Fig. 3(b). Pine Island and Dotson melt are similar to shipboard observations (Naughten et al., 2022), but Thwaites melt rates are much lower than other published results (e.g., Seroussi et al., 2017). The remaining panels (as labeled) show melt difference relative to **baseline** for the other experiments under the various ice shelves. Of all

shelves, Thwaites sees the strongest proportional response in the **runoff** experiment due to its low baseline melt (Fig. 3(b)), with a marginal increase when runoff is increased in **hi runoff**, and similar is seen for Pine Island. At Dotson and Crosson shelves, the melt increase in **runoff** is substantial (a time-mean of 5.3 Gt/a, as compared to 9.4 Gt/a for Thwaites) considering the relatively small runoff input. Getz has a similar runoff magnitude and similar level of increase in melt (though for Getz, this increase is negligible compared to total melt).

From the **runoff** results it is difficult to attribute increased melting at Dotson/Crosson and Getz to either locally (within the cavity) or nonlocally sourced runoff. However, in the **Thwaites only** experiment, where runoff is released only from Thwaites, the melt anomalies under Dotson/Crosson are similar, with a time-mean only 20% smaller than in **runoff**. Meanwhile, the melt under Pine Island is slightly decreased relative to **baseline**. In the **time dependent runoff** experiment, when the runoff reaches its peak in summer 2013, the Thwaites melt anomaly is approximately 2.5 times that of the **runoff** experiment – though at the same time, runoff is nearly an order of magnitude larger. The other ice shelves' melt response to this episodic runoff is minimal, other than under Getz ice shelf where there is a sharp drop in melt (relative to **baseline**) following the pulse in Thwaites runoff.

The **increased** $\mathbf{c}_{fric}$ experiment results in melt anomalies for Pine Island, Dotson/Crosson and Getz that are considerable larger than those due to runoff (while for Thwaites they are of a similar scale). We do not adjust the vertical limits of the corresponding subplots in Fig. 3 to include the **increased** $\mathbf{c}_{fric}$ curve, as the focus for this experiment is Thwaites.

3.2 Sea ice

We examine the effects of ice-shelf freshwater fluxes (both runoff and melt) on effective sea ice thickness, the volume of sea ice per unit area within a grid cell. In this analysis we predominantly compare the **increased** $\mathbf{c}_{fric}$ and **runoff** experiments. While the domain-wide ice-shelf melt differs between these experiments, the collective freshwater volume input (melt plus runoff) from Thwaites is very similar: monthly freshwater input between 2003 and 2015 has a correlation of 0.64 between the experiments, and the 2003-2015 means differ by ∼8%. (As mentioned in Section 2.5, 1995-2003 is considered spinup from the perspective of sea ice influence.) In order to best provide context, results in this section are presented as percent anomalies rather than absolute change.

We examine sea ice on the continental shelf only. Although the model domain extends far beyond the shelf, sea ice cover on-shelf is particularly important because it affects surface process which could have impacts on CDW properties at depth; and in the spring and summer months it controls the light available for photosynthesis. Fig. 4(a) shows mean ice thickness anomalies relative to the **baseline** run over a region with depth less than 1500 m between 235° and 260° longitude (the approximate zonal extent of the summer ice-free region in Naughten et al., 2022). Averaged over the 2003-2015 period, the sea ice anomalies for the both **runoff** and **increased** $\mathbf{c}_{fric}$ are negative, but mean sea ice thinning in **runoff** is larger (2 cm versus 4 mm). Overall the **runoff** anomaly is the most negative in summer, again with greater losses than **increased** $\mathbf{c}_{fric}$. This is made clearer by examining a climatology of mean sea ice thickness anomaly for both experiments (Fig. 4(b)). In the winter (JJA) months, the climatological area-averaged thinning is similar between the two experiments, and is relatively small. In the spring (SON) and summer (DJF) months, the climatologies diverge, with larger thinning in the **runoff** experiment.

The behaviour exhibited in Fig. 4(b) is explored further in Figs. 4(c-f), which show spatial patterns of sea ice anomalies for each experiment, averaged over winter (Figs. 4(c,d)) and summer (Figs. 4(e,f)) months, respectively. As expected from Fig. 4(b) the winter

thinning is relatively small for both experiments. In the summer months, there is fairly large thinning in the **runoff** experiment: ∼10% over most of the continental shelf, which amounts to 5-10 cm. Meanwhile, there is considerable thickening in the **increased** $\mathbf{c}_{fric}$ experiment.

Jourdain et al. (2017) examined impact of ice-shelf melt on sea ice across an ensemble of experiments with different ice-shelf melt parameters (their figure 10(b)). Their result is qualitatively similar to the winter patterns in Figs. 4(c), with strong thinning close to the coast. However, theirs was an annual result, and also used a different ocean model and a different experimental design, so it is not a straightforward comparison.

The basis for comparison between the **runoff** and **increased** $\mathbf{c}_{fric}$ experiments – similar freshwater flux from Thwaites – is not a unique one, and has the consequence that the combined freshwater flux anomaly from Thwaites and Pine Island is considerably larger (by a factor of 2.5) in **increased** $\mathbf{c}_{fric}$ than in **runoff**. Given this disparity, along with the tendency of ice-shelf melt to drive upwelling of warm CDW to the upper ocean, strong sea ice retreat might be expected in **increased** $\mathbf{c}_{fric}$ – yet, the loss of sea ice in the **runoff** experiment is almost 5 times larger. As described in Section 4.2, freshwater flux from Thwaites may play an important role in summer sea ice thinning, motivates our experimental design. In another experiment in which the c_{fric} parameter is tuned such that the combined freshwater flux anomaly from Thwaites and Pine Island is similar to that of **runoff**, the sea ice loss is far less (Supplemental Fig. S5). Thus, our results suggest that freshwater sourced subglacially has a qualitatively different effect on sea ice than water sourced from submarine melt. In the discussion below we explore potential reasons for this.

While our main focus in this section and in the discussion below is on how equal volumes of subglacial runoff and submarine melt can have potentially differing impacts, we briefly note that Fig. 4(a) also shows sea-ice impacts in the **time dependent runoff** experiment. The effect is quite strong, but only for a single season when subglacial runoff is at its peak. The results suggest that episodic runoff can have significant, but short-lived, effects on sea ice thickness.

4 Discussion

4.1 Ice-shelf melt

In the **hi runoff** experiment, runoff from Thwaites is approximately 50% larger than in **runoff**, while the marginal melt increases by 28% (*s.d.* 14%). At the same time, in **time dependent runoff**, the runoff at its largest is ∼13 times larger than in **runoff**, while the summer 2013-2014 melt rate is increased by a factor of 2.5. These results are qualitatively similar to theoretical and modeling studies of runoff-forced plume melting at tidewater glaciers (Jenkins, 2011; Xu et al., 2013; Slater et al., 2015; Cowton et al., 2015), which find sub-linear dependence of melt on runoff flux. While the processes beneath a CDW-forced ice shelf differ from those at a tidewater front, these results suggest similarities in melt response to runoff.

Pine Island and Dotson/Crosson ice shelves exhibit melt responses of similar magnitude in the **runoff** experiment, despite an order of magnitude difference in runoff flux at their respective grounding lines. This suggests a "nonlocal" influence of runoff on the Dotson/Crosson ice shelves, which is reinforced by the **Thwaites only** experiment. The elevated melt under Dotson/Crosson in **runoff** is likely due to a warming found at depth at the Dotson ice-shelf front (Fig. 5(a)), where temperatures below 500 m are increased up to 0.4°C relative to **baseline**. At the same time, there is freshening of 0.02-0.04 psu above 500 m (along with a slight cooling), with little change in salinity at depth except in instances of deep mixing (Fig. 5(b)). A similar signal of surface freshening and warming at depth at the Dotson front is seen in the **increased** $\mathbf{c}_{fric}$ experiment (Figs. 5(c,d)),

coincident with a similar increase in melt (Fig. 3(e)). The effect is stronger than in **runoff**, likely due to the additional melt flux from Pine Island.

The warming at depth coincident with surface freshening suggests a mechanism where increased stratification prevents surface-driven cooling of CDW. Bett et al. (2020) showed that freshwater fluxes from icebergs (crudely represented as an ocean surface freshwater flux) can increase stratification and prevent cooling of CDW due to surface processes at Dotson Ice Shelf – and freshwater sourced from either distal runoff and/or increased ice shelf melt may play a similar role. Meanwhile, the **Thwaites only** experiment sees analogous warming at depth and surface freshening (5(e,f)). There is a smaller freshwater flux, and thus the signal is not as strong, but it reinforces the nonlocal influence of runoff on stratification.

Some warming at depth is seen at the front of Pine Island in the **runoff** and **increased $\mathbf{c}_{fric}$** experiments (Figs. 6(a,c)). However this warming is less consistent than at the Dotson Ice Shelf front, and also interspersed with periods of cooling. Therefore, although Pine Island melt increases in the **runoff** experiment, it is unlikely this is attributable to deep warming (with the exception of 2013/2014, discussed below), but rather that melt is locally runoff-forced. On the other hand, cooling at depth is seen in **Thwaites only** as well, and could be the cause of the negative Pine Island melt anomaly in that experiment, which is not "hidden" by a local runoff source.

The most pronounced warming at depth for Pine Island ($\sim$0.4°C) is seen in 2013-2014, a period during which there is a cool bias with respect to observations in **baseline** (Naughten et al., 2021). The warming is likely responsible for the increase in melt seen in the runoff experiments. (In the **increased $\mathbf{c}_{fric}$** experiment, any increase due to ocean properties is overwhelmed by the melt parameter change). It is possible that, similarly to Dotson, surface freshening due to runoff and/or melt increases stratification and prevents surface-driven cooling of CDW. The 2013/2014 warming is seen in the **runoff**, **Thwaites only** and **increased $\mathbf{c}_{fric}$** experiments (Figs. 6(a,c,e)), suggesting that it is driven by freshwater flux regardless of the source.

It is not clear why runoff forcing at Thwaites alone would drive a cooling at depth in front of Pine Island. Yoon et al. (2022) show evidence of a double-gyre system of circulation in front of Pine Island ice shelf which controls the conditions within the cavity, and argue that a change in the position of the calving front can alter this double-gyre pattern and hence the cavity conditions. It is possible that fresh water input from Thwaites ice shelf can impact this double-gyre circulation as well, but further investigation is needed.

4.2 Sea ice reduction

The above discussion of nonlocal effects of runoff on ice-shelf melt suggests impacts of runoff on hydrography are due to their contribution to fresh water fluxes – such that, for instance, an increase in ice-shelf melt may have similar effects to a runoff increase of similar magnitude. This does not appear to be the case for sea ice, as an increase in freshwater flux due to runoff has a bigger effect on summer sea ice than a much larger increase due to melt alone.

Jourdain et al. (2017) suggest that increased overturning in response to elevated melt can bring more heat to ice-shelf fronts, where it is brought to the surface through mixing and vertical advection. For Pine Island, we see increased overturning in response to both melt and runoff (Fig. 7(a,c)). Moreover the responses are similar in terms of overturning per unit of freshwater flux: in the non-runoff experiments, the best-fit linear relationship between melt and overturning yields a slope $m = 0.0014$ Sv per Gt/a of melt (R^2=0.7). A similar regression is not carried out for runoff, as runoff volume flux is held constant. However in the **runoff** experiment, the mean 1995-2015 increase of Pine Is-

land melt relative to **baseline** is about 4 Gt/a, giving a combined release of ∼7 Gt/a released into the cavity (runoff plus additional melt). From the above melt-overturning relationship, the predicted increase in overturning in **runoff** is thus ∼0.01 Sv, whereas an increase of 0.014 Sv is seen (Fig. 7(c)). In the Thwaites cavity there is a weak relationship between melt and overturning (Fig. 7(a); $m = 0.0019$, R^2=0.29), and a calculation similar to the above for Pine Island predicts an increase in ∼0.027 Sv in response to the presence of runoff. Meanwhile, a mean increase of ∼0.1 Sv is seen (Fig. 7(c)).

The above comparisons suggest that, for the Pine Island cavity, the response in overturning is agnostic to the source of fresh water; while under Thwaites, runoff has a distinct effect on overturning. The reasons for this are unclear. It could be that under Pine Island, the runoff and its induced melt is a relatively small perturbation to the background state, which is not the case for Thwaites, hence the qualitatively different response. Further investigation of the mechanism of overturning, with a range of model types and resolution, is needed.

Nevertheless, we examine the effects of this increased overturning – and the associated heat transport to the upper ocean – on temperatures in the upper 400 m, averaged over the region indicated by the mid-shelf rectangular box in Figs. 4(e,f). This region is chosen because of its alignment with the Amundsen Polynya, which supports extremely high rates of productivity in summer months due to the relative availability of light (Yager et al., 2012). The results are presented as a Hovmöller diagrams for the **runoff**, **increased** c_{fric}, and **Thwaites only** experiments (Figs. 8(a,c,e), respectively). In the runoff experiment, there is a strong seasonal surface warming (relative to **baseline**) that extends down to ∼50-100 m in most years, as well as a periodic warming of approximately 0.1°C which extends from ∼100-400 m. The strong surface warming is likely due to increased radiative heating from reduced sea ice cover, and as such is a result rather than a cause of lowered sea ice. The deeper warming, on the other hand, likely arises from upwelling and export of CDW from within the ice-shelf cavity, rather than vertical mixing. It can be seen from salinity Hovmöller diagrams for the same location (Fig. 8(b,d,e)) that vertical mixing of seasonal surface freshening does not extend to these depths; rather, winter mixing erodes the signal at depth.

We propose that relatively warm waters brought to mid-depths by ice-shelf overturning in the **runoff** experiment occupy large parts of the continental shelf, and that mixing over the upper 100-200 m resulting from winter brine rejection brings this heat to the near-surface, where it limits sea ice growth in later seasons. The temperature elevation is very minor (<0.1°C) but enough to have an effect on sea ice – which may be amplified by other feedbacks in the ice/ocean system such as radiative heating. In the **increased** $\mathbf{c}_{fric}$ experiment, in which Thwaites overturning is relatively weak, this mid-depth warming at 100-400 m is mostly absent (Fig. 8(e)). There is still a small surface warming signal due to there being some summer ice loss in this region (Fig. 4(f)), though to a lesser extent than in **runoff**. In the **Thwaites only** experiment, there is again mid-depth warming (Fig. 8(e)), but it is less persistent than in **runoff**. We therefore attribute the loss of summer sea ice in the **runoff** experiment to runoff-driven overturning under Thwaites ice shelf, and to a lesser extent under Pine Island ice shelf. Meanwhile, increased melt due to an artificially increased frictional drag parameter does not have a similar effect despite similar volumes of fresh water flux.

We further examine the role of water transformation under the ice shelves by considering temperature-salinity (T-S) diagrams under Pine Island and Thwaites for June 2011 (Fig. 9), a month in which total Thwaites freshwater flux is very similar between the **runoff** and **increased** $\mathbf{c}_{fric}$ experiments. While sea ice reduction is largest in the summer months (*cf.* Fig. 4), choosing a winter month removes water masses resulting from surface processes which complicate the diagram. Fig. 9(a) overlays the T-S diagram from **baseline** on that of **runoff** and **increased** $\mathbf{c}_{fric}$, restricted to Pine Island. Here a locus of points can be seen indicative of water mass transformation due to ice-shelf melt

(Gade, 1979). Little difference can be seen, with the exception of additional melt in the **increased $\mathbf{c}_{fric}$** causing an extension of this locus of points. Fig. 9(c) compares the experiments under the region of Thwaites west of 254° longitude. In the **runoff** experiment there appears to be a freshening of water masses originating at a density of ∼1027.8 kg/m^3, the density of the grounding line cell with the largest runoff flux – and such a feature is absent from the part of Thwaites east of the runoff entry (Fig. 9(b)). The effect is relatively minor, but could result in slightly warmed buoyant water masses that can cause upper-ocean warming on the continental shelf.

The effects are far more obvious in the **time dependent runoff** experiment. Fig. 9(d) plots a similar T-S diagram for western Thwaites for June 2013, when runoff is at its peak. There is a strong freshening where runoff enters the cavity, and this results in warmer waters, relative to the other experiments, at a range of densities. To put another way: since runoff freshens water without phase transformation, it does so without transforming along the relatively steep Gade line. Submarine melting of an ice shelf consumes latent heat, but for subglacial meltwater this heat is consumed beneath the ice sheet instead.

Still, this effective warming within Thwaites cavity alone does not explain the relative reduction in sea ice. However, the observations of Zheng et al. (2021) suggest that in the summer months, melt-freshened water exiting ice shelves can spread tens of kilometers or more away from the coast. Examination of our melt water tracer (Supplemental Fig. S4) suggests similar behaviour in our model.

Thus it is plausible that, for a given density, runoff leads to warming, and that warming signal spreads across the shelf, giving rise to the mid-depth warming in Fig. 5(e). There may additionally be a positive feedback between ice loss and surface radiative heating. Meanwhile, Zheng et al. (2021) also suggests that in the winter, upwelled waters remain close to the coast; this is consistent with our modeled pattern of coastally-intensified thinning in the winter (Fig. 4(c,d)).

We briefly note that the melt-overturning relationships in Fig. 7(a,b) give regression slopes roughly twice of those found by Jourdain et al. (2017), and a far weaker linear relationship for Thwaites. However, it is a different model with different forcings, and their results are time-averaged across an ensemble of model parameters (whereas ours are monthly). Moreover our overturning calculation is distinct (though similar) to that study. Given that our model is of similar resolution, complexity and scale, we do not feel these differences diminish our findings.

4.3 Wider significance

While the summer sea ice reduction we see as a result of runoff (mean 3 cm, but up to ∼15 cm in places) is small compared to mean DJF sea ice thickness on the shelf (mean 70 cm), it is still significant. Reduction of sea ice is associated with stronger stratification, which can prevent convection and erosion of warm CDW. Sea ice cover is a major factor in biological productivity of the seasonal Pine Island and Amundsen Sea Polynyas, two of the most productive seasonal polynyas in Antarctica (Arrigo et al., 2012), and reduced sea ice thickness could modify productivity and carbon cycling.

The results are also significant because of how little is known about Antarctic subglacial hydrology. The experiments in this study simply represent different estimates of patterns of basal ice melt, and of spatiotemporal patterns of runoff. Steady runoff rates are derived based on estimates of geothermal flux, which could be over- or underestimates.

The results of our **time dependent runoff** experiment suggest that when runoff is episodic, the proportionate melt increase may be much smaller than the proportionate increase in runoff. As the runoff flux is expected to be the same in the long term,

and hence the increase in runoff is inversely proportional to the period during which runoff occurs, this implies that the long-term impact of runoff on ice shelves is likely larger when runoff is sustained, rather than episodic. Meanwhile, episodic runoff has a strong impact on summer sea ice in our results. Observations of lake drainages (Smith et al., 2017; Malczyk et al., 2020; Hoffman et al., 2020) suggest episodic drainage does occur. Moreover, if the Thwaites catchment were to transition from episodic to steady runoff in the future, this could have significant effects on ice-shelf melt and sea-ice variability.

The mechanism that we suggest above – that runoff leads to warmer sub-ice shelf water masses than an equivalent volume of submarine melt – is not specific to the Amundsen Sea Embayment. In other areas in Antarctica with strong subglacial activity and warm water under ice shelves (e.g., Dow et al., 2020), runoff likely has similar effects. As mentioned above, runoff effectively transfers latent heat from the ice sheet to the ocean by adding buoyancy without drawing heat content. With Antarctic-wide subglacial melt estimated to be ∼65 Gt/a (Pattyn, 2010), this is equivalent to 0.7 TW. In other words, an ocean model which seeks to reproduce fresh water flux from ice shelves without runoff will be deficient by this amount. While this is a small value relative to the estimated heat transported to the shelf from the deep ocean (∼20 TW, Palóczy et al., 2018), thermal signals associated with deep melting or runoff are likely to reach the upper ocean. Thus, subglacial runoff effectively represents a heat source not currently accounted for in ocean models.

5 Conclusions

We carry out a set of regional ocean simulations of the Amundsen Sea Embayment, some of which are forced by subglacial runoff with varying magnitudes and temporal character. Subglacial runoff is found to impact ice-shelf melt, both due to local and non-local effects. Episodic runoff leads to an increase in melt, but one that is not commensurate with the increase in runoff volume, based on expectations from steady simulations.

When normalising for the input of fresh water to the ocean, the impact of runoff on sea ice is qualitatively different than that of increased ice-shelf melt. This sea-ice loss is coincident with an apparent warming under ice shelves. We propose this warming is driven by freshening due to runoff, and that the warming signal is brought to the surface, causing sea-ice reduction over the continental shelf in the summer months.

The results suggest that Antarctic runoff is a potentially important source freshwater (and heat) not represented in regional and continental ocean models of Antarctica. Progress is impeded by lack of knowledge about Antarctica's subglacial environment. However, as direct observation of ice-shelf cavities and grounding lines increase (e.g., Begeman et al., 2018, 2020), this could lead to better quantification and deeper understanding of subglacial impact on the Southern Ocean.

6 Open Research

The MITgcm (mitgcm.org), checkpoint 67v was used for this study. The source is freely available for download (`https://github.com/MITgcm/MITgcm`). The zenodo archive 10.5281/zenodo.7713349 contains (i) all modified source code pertaining to the implementation of runoff in MITgcm (folder modified_code/), (ii) all experiment-specific code and inputs (input/ and expt_code/), and (iii) all relevant model output (in output/).

Acknowledgments

DNG and MGW acknowledge support from UKRI grant NE/S006796/1 and the European Space Agency funding projects 4000128611/19/I-DT, 4D Antarctica and Digital Twin Antarctica. AGT acknowledges support from UKRI doctoral training partnership

grant NE/L002558/1. The ocean simulations were run on ARCHER2 (https://www.archer2.ac.uk/), requiring approximately 1700 CU (including failed and re-run experiments), with an estimated CO_2 cost of ∼280 kg (https://frost-group.github.io).

References

Adusumilli, S., Fricker, H. A., Medley, B., Padman, L., & Siegfried, M. R. (2020). Interannual variations in meltwater input to the southern ocean from antarctic ice shelves. *Nature geoscience*, *13*(9), 616–620. doi: 10.1038/s41561-020-0616-z

Arrigo, K. R., Lowry, K. E., & van Dijken, G. L. (2012). Annual changes in sea ice and phytoplankton in polynyas of the amundsen sea, antarctica. *Deep Sea Research Part II: Topical Studies in Oceanography*, *71*, 5–15. doi: 10.1016/j.dsr2.2012.03.006

Begeman, C. B., Tulaczyk, S., Padman, L., King, M., Siegfried, M. R., Hodson, T. O., & Fricker, H. A. (2020). Tidal pressurization of the ocean cavity near an antarctic ice shelf grounding line. *Journal of Geophysical Research: Oceans*, *125*(4), e2019JC015562. doi: 10.1029/2019JC015562

Begeman, C. B., Tulaczyk, S. M., Marsh, O. J., Mikucki, J. A., Stanton, T. P., Hodson, T. O., ... King, M. A. (2018). Ocean stratification and low melt rates at the ross ice shelf grounding zone. *Journal of Geophysical Research: Oceans*, *123*(10), 7438–7452. doi: 10.1029/2018JC013987

Bett, D. T., Holland, P. R., Naveira Garabato, A. C., Jenkins, A., Dutrieux, P., Kimura, S., & Fleming, A. (2020). The impact of the amundsen sea freshwater balance on ocean melting of the west antarctic ice sheet. *Journal of Geophysical Research: Oceans*, *125*(9), e2020JC016305. doi: 10.1029/2020JC016305

Colgan, W., MacGregor, J. A., Mankoff, K. D., Haagenson, R., Rajaram, H., Martos, Y. M., ... Kjeldsen, K. K. (2021, February). Topographic Correction of Geothermal Heat Flux in Greenland and Antarctica. *Journal of Geophysical Research (Earth Surface)*, *126*(2), e05598. doi: 10.1029/2020JF005598

Cowton, T., Slater, D., Sole, A., Goldberg, D., & Nienow, P. (2015). Modeling the impact of glacial runoff on fjord circulation and submarine melt rate using a new subgrid-scale parameterization for glacial plumes. *Journal of Geophysical Research: Oceans*, *120*(2), 796–812. doi: 10.1002/2014JC010324

Cowton, T., Sole, A., Nienow, P., Slater, D., Wilton, D., & Hanna, E. (2016). Controls on the transport of oceanic heat to kangerdlugssuaq glacier, east greenland. *Journal of Glaciology*, *62*(236), 1167–1180. doi: 10.1017/jog.2016.117

Cuffey, K., & Paterson, W. S. B. (2010). *The physics of glaciers* (4th ed.). Oxford: Butterworth Heinemann.

Dansereau, V., Heimbach, P., & Losch, M. (2014). Simulation of subice shelf melt rates in a general circulation model: Velocity-dependent transfer and the role of friction. *Journal of Geophysical Research: Oceans*, *119*(3), 1765–1790. doi: 10.1002/2013JC008846

Dow, C., McCormack, F., Young, D., Greenbaum, J., Roberts, J., & Blankenship, D. (2020). Totten glacier subglacial hydrology determined from geophysics and modeling. *Earth and Planetary Science Letters*, *531*, 115961. doi: 10.1016/j.epsl.2019.115961

Drews, R., Pattyn, F., Hewitt, I. J., Ng, F. S. L., Berger, S., Matsuoka, K., ... Neckel, N. (2017, May). Actively evolving subglacial conduits and eskers initiate ice shelf channels at an Antarctic grounding line. *Nature Communications*, *8*, 15228. doi: 10.1038/ncomms15228

Favier, L., Durand, G., Cornford, S. L., Gudmundsson, G. H., Gagliardini, O., Gillet-Chaulet, F., ... Brocq, A. M. L. (2014). Retreat of Pine Island Glacier controlled by marine ice-sheet instability. *Nature Climate Change*, *4*, 117–121. doi: 10.1038/nclimate2094

Gade, H. G. (1979). Melting of ice in sea water: A primitive model with application to the antarctic ice shelf and icebergs. *Journal of Physical Oceanography*, *9*(1), 189–198. doi: 10.1175/1520-0485(1979)009⟨0189:MOIISW⟩2.0.CO;2

Goldberg, D. N., Gourmelen, N., Kimura, S., Millan, R., & Snow, K. (2019). How accurately should we model ice shelf melt rates? *Geophysical Research Letters*, *46*(1), 189–199. doi: http://dx.doi.org/10.1029/2018GL080383

Goldberg, D. N., & Heimbach, P. (2013). Parameter and state estimation with a time-dependent adjoint marine ice sheet model. *The Cryosphere*, *7*(6), 1659–1678. doi: 10.5194/tc-7-1659-2013

Goldberg, D. N., & Holland, P. (2022). The relative impacts of initialisation and climate forcing in coupled ice sheet-ocean modelling application to pope, smith and kohler glaciers. *Journal of Geophysical Research: Earth Surface*, e2021JF006570. doi: 10.1029/2021JF006570

Hager, A. O., Hoffman, M. J., Price, S. F., & Schroeder, D. M. (2022). Persistent, extensive channelized drainage modeled beneath thwaites glacier, west antarctica. *The Cryosphere*, *16*(9), 3575–3599. Retrieved from `https://tc.copernicus.org/articles/16/3575/2022/` doi: 10.5194/tc-16-3575-2022

Hoffman, A. O., Christianson, K., Shapero, D., Smith, B. E., & Joughin, I. (2020). Brief communication: Heterogenous thinning and subglacial lake activity on thwaites glacier, west antarctica. *The Cryosphere*, *14*(12), 4603–4609. doi: 10.5194/tc-14-4603-2020

Jenkins, A. (2011). Convection-driven melting near the grounding lines of ice shelves and tidewater glaciers. *Journal of Physical Oceanography*, *41*(12), 2279–2294. doi: 10.1175/JPO-D-11-03.1

Joughin, I., Smith, B. E., & Medley, B. (2014). Marine ice sheet collapse potentially under way for the Thwaites Glacier Basin, West Antarctica. *Science*, *344*(6185), 735-738. doi: 10.1126/science.1249055

Joughin, I., Tulaczyk, S., Bamber, J. L., Blankenship, D., Holt, J. W., Scambos, T., & Vaughan, D. G. (2009). Basal conditions for Pine Island and Thwaites Glaciers, West Antarctica, determined using satellite and airborne data. *Journal of Glaciology*, *55*, 245–257. doi: 10.3189/002214309788608705

Jourdain, N. C., Mathiot, P., Merino, N., Durand, G., Le Sommer, J., Spence, P., ... Madec, G. (2017). Ocean circulation and sea-ice thinning induced by melting ice shelves in the a mundsen s ea. *Journal of Geophysical Research: Oceans*, *122*(3), 2550–2573. doi: 10.1002/2016JC012509

Kimura, S., Adrian, J., Heather, R., R., H. P., M., A. K., B., W. D., ... Pierre, D. (2017). Oceanographic Controls on the Variability of Ice-Shelf Basal Melting and Circulation of Glacial Meltwater in the Amundsen Sea Embayment, Antarctica. *Journal of Geophysical Research: Oceans*, *122*(12), 10131-10155. doi: 10.1002/2017JC012926

Le Brocq, A. M., Payne, A. J., Siegert, M. J., & Alley, R. B. (2009, January). A subglacial water-flow model for West Antarctica. *Journal of Glaciology*, *55*(193), 879-888. doi: 10.3189/002214309790152564

Le Brocq, A. M., Ross, N., Griggs, J. A., Bingham, R. G., Corr, H. F., Ferraccioli, F., ... others (2013). Evidence from ice shelves for channelized meltwater flow beneath the antarctic ice sheet. *Nature Geoscience*, *6*(11), 945–948. doi: 10.1038/ngeo1977

Locarnini, M., Mishonov, A., Baranova, O., Boyer, T., Zweng, M., Garcia, H., ... Smolyar, I. (2018). World ocean atlas 2018, volume 1: Temperature [Report]. *NOAA Atlas*. Retrieved from `https://archimer.ifremer.fr/doc/00651/76338/` doi: https://archimer.ifremer.fr/doc/00651/76339/

Losch, M. (2008). Modeling ice shelf cavities in a z coordinate ocean general circulation model. *Journal of Geophysical Research: Oceans*, *113*(C8), C08043. doi: 10.1029/2007JC004368

Losch, M., Menemenlis, D., Campin, J.-M., Heimbach, P., & Hill, C. (2010, January). On the formulation of sea-ice models. Part 1: Effects of different solver implementations and parameterizations. *Ocean Modelling*, *33*(1), 129-144. doi: 10.1016/j.ocemod.2009.12.008

Malczyk, G., Gourmelen, N., Goldberg, D., Wuite, J., & Nagler, T. (2020). Repeat subglacial lake drainage and filling beneath thwaites glacier. *Geophysical Research Letters*, *47*(23), e2020GL089658. doi: 10.1029/2020GL089658

Marshall, J., Hill, C., Perelman, L., & Adcroft, A. (1997). Hydrostatic, quasi-hydrostatic, and nonhydrostatic ocean modeling. *Journal of Geophysical Research: Oceans*, *102*(C3), 5733–5752. doi: 10.1029/96JC02776

Martos, Y. M., Catalán, M., Jordan, T. A., Golynsky, A., Golynsky, D., Eagles, G., & Vaughan, D. G. (2017, November). Heat Flux Distribution of Antarctica Unveiled. *Geophys. Res. Lett*, *44*(22), 11417–11426. doi: 10.1002/2017GL075609

Mathiot, P., Jenkins, A., Harris, C., & Madec, G. (2017). Explicit representation and parametrised impacts of under ice shelf seas in the z coordinate ocean model nemo 3.6. *Geoscientific Model Development*, *10*(7), 2849–2874. doi: 10.5194/gmd-10-2849-2017

Merino, N., Le Sommer, J., Durand, G., Jourdain, N. C., Madec, G., Mathiot, P., & Tournadre, J. (2016). Antarctic icebergs melt over the southern ocean: Climatology and impact on sea ice. *Ocean Modelling*, *104*, 99–110. doi: 10.1016/j.ocemod.2016.05.001

Mernild, S., Howat, I. M., Ahn, Y., Liston, G. E., Steffen, K., Jakobsen, B. H., ... van As, D. (2010, October). Freshwater flux to Sermilik Fjord, SE Greenland. *The Cryosphere*, *4*(4), 453-465. doi: 10.5194/tc-4-453-2010

Mernild, S., Liston, G. E., Steffen, K., & Chylek, P. (2010, April). Meltwater flux and runoff modeling in the ablation area of Jakobshavn Isbræ, West Greenland. *Journal of Glaciology*, *56*(195), 20-32. doi: 10.3189/002214310791190794

Morlighem, M., Rignot, E., Binder, T., Blankenship, D., Drews, R., Eagles, G., ... others (2020). Deep glacial troughs and stabilizing ridges unveiled beneath the margins of the Antarctic ice sheet. *Nature Geoscience*, *13*(2), 132–137. doi: http://dx.doi.org/10.1038/s41561-019-0510-8

Motyka, R. J., Dryer, W. P., Amundson, J., Truffer, M., & Fahnestock, M. (2013). Rapid submarine melting driven by subglacial discharge, leconte glacier, alaska. *Geophysical Research Letters*, *40*(19), 5153–5158. doi: 10.1002/grl.51011

Nakayama, Y., Cai, C., & Seroussi, H. (2021, September). Impact of Subglacial Freshwater Discharge on Pine Island Ice Shelf. *Geophys. Res. Lett*, *48*(18), e93923. doi: 10.1029/2021GL093923

Naughten, K. A., De Rydt, J., Rosier, S. H., Jenkins, A., Holland, P. R., & Ridley, J. K. (2021). Two-timescale response of a large Antarctic ice shelf to climate change. *Nature communications*, *12*(1), 1–10. doi: http://dx.doi.org/10.1038/s41467-021-22259-0

Naughten, K. A., Holland, P. R., Dutrieux, P., Kimura, S., Bett, D. T., & Jenkins, A. (2022, March). Simulated Twentieth-Century Ocean Warming in the Amundsen Sea, West Antarctica. *Geophys. Res. Lett*, *49*(5), e94566. doi: 10.1029/2021GL094566

Palóczy, A., Gille, S. T., & McClean, J. L. (2018). Oceanic heat delivery to the antarctic continental shelf: Large-scale, low-frequency variability. *Journal of Geophysical Research: Oceans*, *123*(11), 7678–7701. doi: 10.1029/2018JC014345

Pattyn, F. (2010, July). Antarctic subglacial conditions inferred from a hybrid ice sheet/ice stream model. *Earth and Planetary Science Letters*, *295*(3-4), 451-461. doi: 10.1016/j.epsl.2010.04.025

Rignot, E., Mouginot, J., & Scheuchl, B. (2011). Ice flow of the Antarctic Ice Sheet. *Science*, *333*(6048), 1427-1430. doi: 10.1126/science.1208336

Schroeder, D. M., Blankenship, D. D., & Young, D. A. (2013). Evidence for a water system transition beneath thwaites glacier, west antarctica. *Proceedings of the National Academy of Sciences*, *110*(30), 12225-12228. Retrieved from `http://www.pnas.org/content/110/30/12225.abstract` doi: 10.1073/pnas.1302828110

Seroussi, H., Nakayama, Y., Larour, E., Menemenlis, D., Morlighem, M., Rignot, E., & Khazendar, A. (2017). Continued retreat of thwaites glacier, west antarctica, controlled by bed topography and ocean circulation. *Geophysical Research Letters*, 6191—6199. doi: 10.1002/2017GL072910

Silvano, A., Rintoul, S. R., Peña-Molino, B., Hobbs, W. R., van Wijk, E., Aoki, S., ... Williams, G. D. (2018). Freshening by glacial meltwater enhances melting of ice shelves and reduces formation of antarctic bottom water. *Science advances*, *4*(4), eaap9467. doi: 10.1126/sciadv.aap9467

Slater, D., Goldberg, D. N., Nienow, P. W., & Cowton, T. R. (2016). Scalings for submarine melting at tidewater glaciers from buoyant plume theory. *Journal of Physical Oceanography*, *46*(6), 1839–1855. doi: 10.1175/JPO-D-15-0132.1

Slater, D., Nienow, P., Cowton, T., Goldberg, D., & Sole, A. (2015). Effect of near-terminus subglacial hydrology on tidewater glacier submarine melt rates. *Geophysical Research Letters*, *42*(8), 2861–2868. doi: 10.1002/2014GL062494

Slater, D., Straneo, F., Das, S., Richards, C., Wagner, T., & Nienow, P. (2018). Localized plumes drive front-wide ocean melting of a greenlandic tidewater glacier. *Geophysical Research Letters*, *45*(22), 12–350. doi: 10.1029/2018GL080763

Smith, B. E., Gourmelen, N., Huth, A., & Joughin, I. (2017). Connected subglacial lake drainage beneath thwaites glacier, west antarctica. *The Cryosphere*, *11*(1), 451–467. doi: :10.5194/tc-11-451-2017

Van Liefferinge, B., & Pattyn, F. (2013). Using ice-flow models to evaluate potential sites of million year-old ice in Antarctica. *Climate of the Past Discussions*, *9*(3). doi: http://dx.doi.org/10.5194/cp-9-2335-2013

Verdy, A., & Mazloff, M. R. (2017, September). A data assimilating model for estimating Southern Ocean biogeochemistry. *Journal of Geophysical Research (Oceans)*, *122*(9), 6968-6988. doi: 10.1002/2016JC012650

Xu, Y., Rignot, E., Fenty, I., Menemenlis, D., & Flexas, M. M. (2013). Subaqueous melting of store glacier, west greenland from three-dimensional, high-resolution numerical modeling and ocean observations. *Geophysical Research Letters*, *40*(17), 4648–4653. doi: 10.1002/grl.50825

Yager, P. L., Sherrell, R. M., Stammerjohn, S. E., Alderkamp, A.-C., Schofield, O., Abrahamsen, E. P., ... others (2012). Aspire: the amundsen sea polynya international research expedition. *Oceanography*, *25*(3), 40–53. doi: 10.5670/oceanog.2012.73

Yoon, S.-T., Lee, W. S., Nam, S., Lee, C.-K., Yun, S., Heywood, K., ... others (2022). Ice front retreat reconfigures meltwater-driven gyres modulating ocean heat delivery to an antarctic ice shelf. *Nature communications*, *13*(1), 1–8. doi: 10.1038/s41467-022-27968-8

Zheng, Y., Heywood, K. J., Webber, B. G., Stevens, D. P., Biddle, L. C., Boehme, L., & Loose, B. (2021). Winter seal-based observations reveal glacial meltwater surfacing in the southeastern amundsen sea. *Communications Earth & Environment*, *2*(1), 1–9. doi: 10.1038/s43247-021-00111-z

Zweng, M., Reagan, J., Seidov, D., Boyer, T., Locarnini, M., Garcia, H., ... Smolyar, I. (2019). World ocean atlas 2018, volume 2: Salinity [Report]. *NOAA Atlas*. Retrieved from `https://archimer.ifremer.fr/doc/00651/76339/` doi: https://archimer.ifremer.fr/doc/00651/76339/

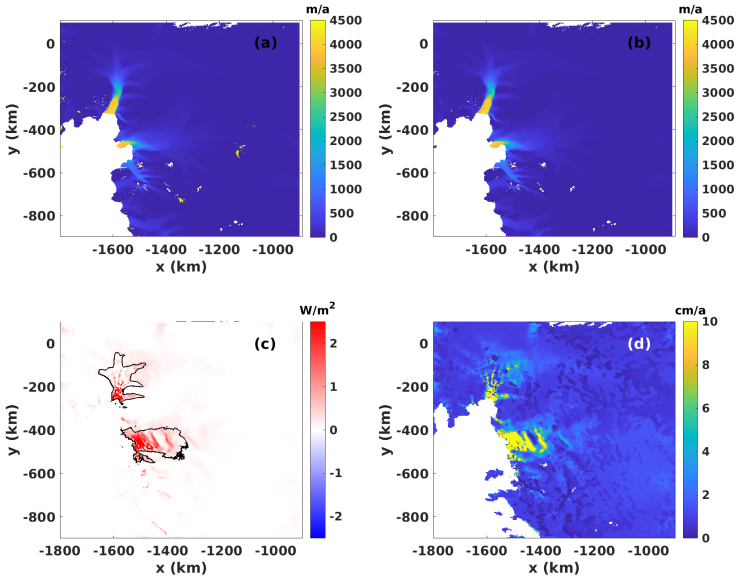

Figure 1. An overview of how the basal dissipation term of Eq. 1 is derived using an ice-sheet model. (a) MEaSUREs ice speed. (b) modeled ice speed. (c) Frictional heating corresponding to the model solution in (d) Calculated melt rate in **runoff** experiment.

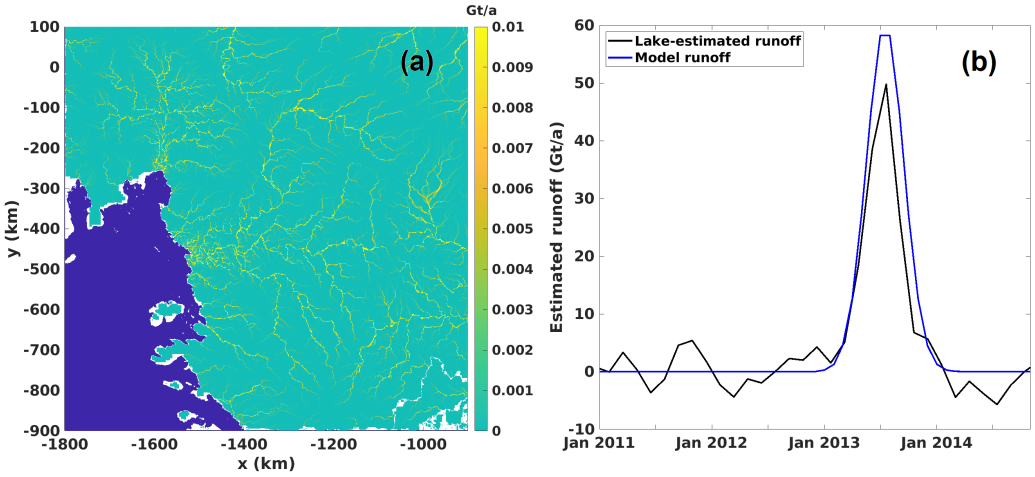

Figure 2. (a) Routing flux from Le Brocq et al. (2009) model calculation, with color range saturated to show entire network. Blue pixels represent ocean according to the BedMachine product, and white pixels are where the computation could not be carried out. (b) The runoff forcing for the **time dependent runoff** experiment. Black curve: combined rate of observed volume change under the four mapped lakes under Thwaites. Blue curve: a gaussian profile which is an idealisation of the observed change. The blue curve is zero prior to January 2013.

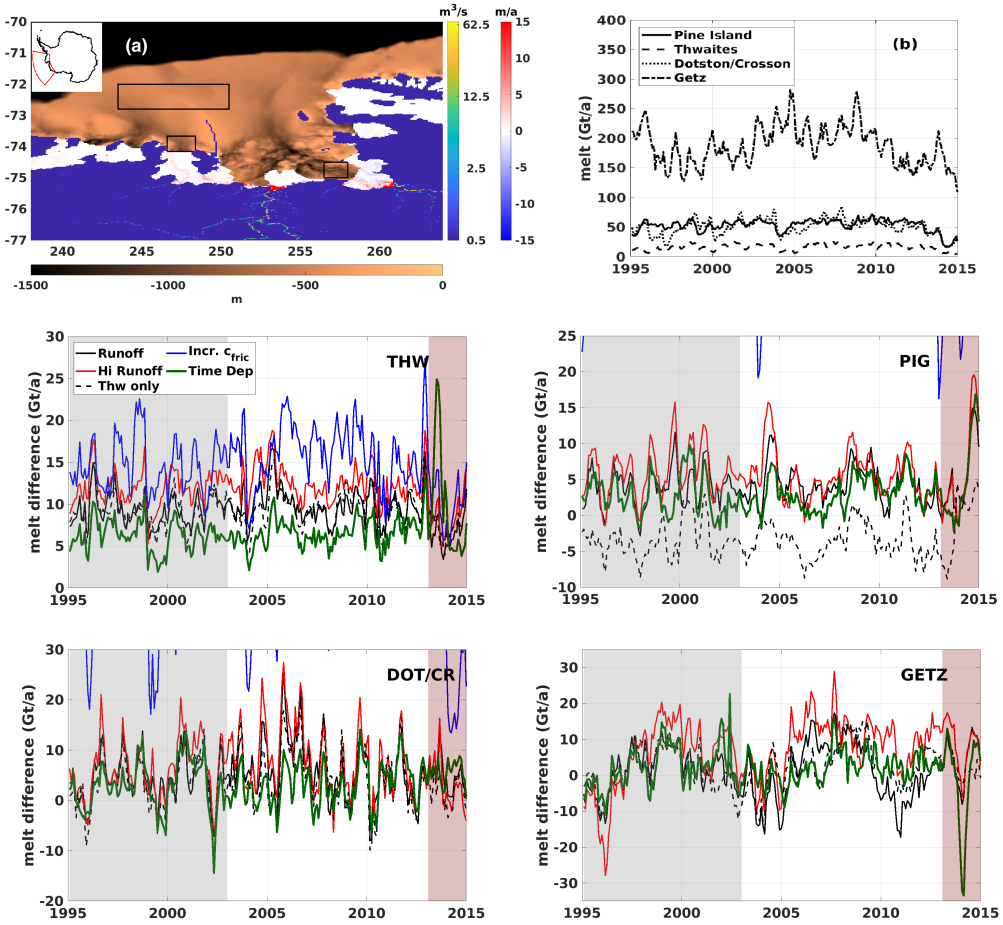

Figure 3. (a) A section of the model domain containing the continental shelf and modeled ice shelves (full domain is given in the inset), with ocean bathymetry as copper shading. Red-blue shading shows the time-mean change in melt in the **runoff** experiment relative to **baseline**. Where ice is grounded, the routing solution corresponding to the **runoff** experiment is shown on a logarithmic scale. The black boxes indicate the regions used for the Hovmöller diagrams in Figs. 5, 6, and 8. (b) Time series of monthly melt rate corresponding to Pine Island, Thwaites, Dotson/Crosson and Getz ice shelves in the **baseline** run. (c)-(f) monthly difference in melt rate relative to **baseline** for Thwaites, Pine Island, Dotson/Crosson, and Getz, respectively, in each of the perturbation experiments discussed in Section 2.5. Gray shaded regions represent the "spinup" period over which the continental shelf adjusts to freshwater input, and the red shaded regions indicate where runoff in the **time dependent runoff** experiment is nonzero.

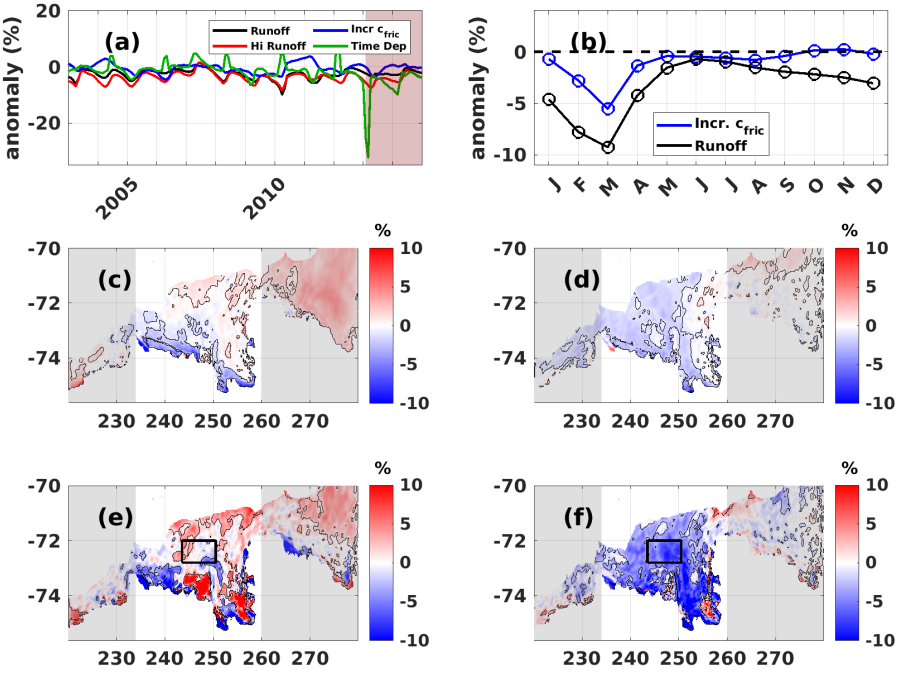

Figure 4. (a) Monthly change in mean effective sea ice thickness on the continental shelf, relative to **baseline**, in the experiments shown. The ocean-model spinup period is excluded, and the red-shaded period indicates where time-dependent runoff is nonzero. Results in (b)-(f) correspond to the period shown. (b) A monthly climatology of mean effective sea ice thickness relative to **baseline** in the **runoff** and **increased** $\mathbf{c}_{fric}$ experiments. (c) Change in winter (JJA) sea ice effective thickness relative to **baseline** in the **increased** $\mathbf{c}_{fric}$ experiment. Black contours indicate 95% significance, based on a t-statistic with degrees of freedom equal to the number of months. (d) Similar to (c) for **runoff**. (e,f) similar to (c,d) for summer sea ice thickness.

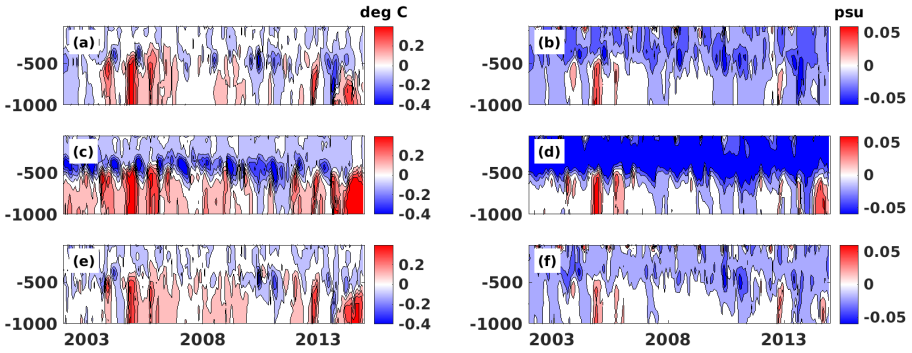

Figure 5. Left column: Hovmöller diagrams of temperature anomaly at depth relative to the **baseline** experiment, width-averaged over the box at the Pine Island front in Fig. 3(a), for the (a) **runoff** experiment, (c) **increased** $\mathbf{c}_{fric}$ experiment, and (e) **increased** $\mathbf{c}_{fric}$ experiment. Right column: as in the left column but for salinity.

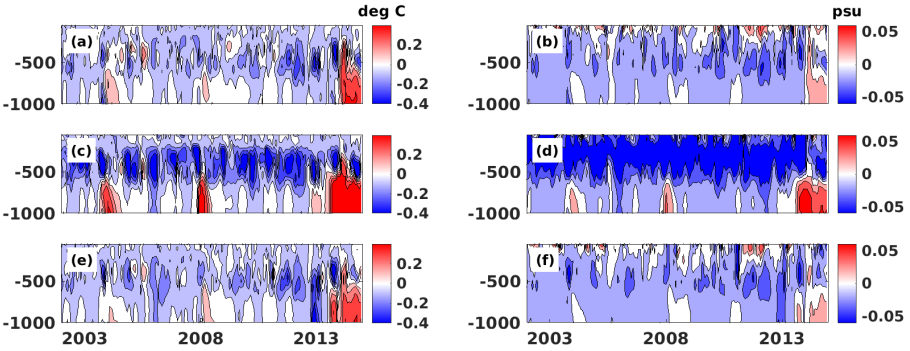

Figure 6. As in Fig. 5, but for the Dotson ice shelf front box in Fig. 3(a).

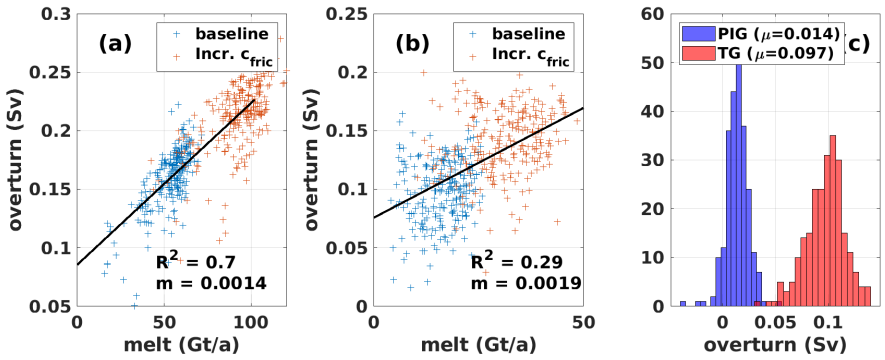

Figure 7. (a) Plot of calculated overturning versus ice-shelf melt for Pine Island in the non-runoff experiments. Each data point represents a different month between 1995 and 2015. (b) Similar to (a) for Thwaites. (c) Histograms of increase in overturning (relative to **baseline**) for Pine Island and Thwaites in the **runoff** experiment. The samples represent monthly values between 1995 and 2015.

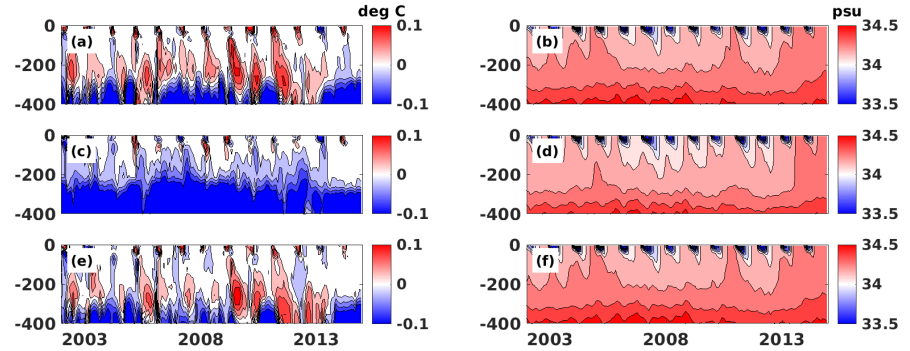

Figure 8. As in Fig. 5, but for the mid-continental shelf box in Figs. 3(a) and 4(e,f), and salinities in the right column as absolute rather than anomalies.

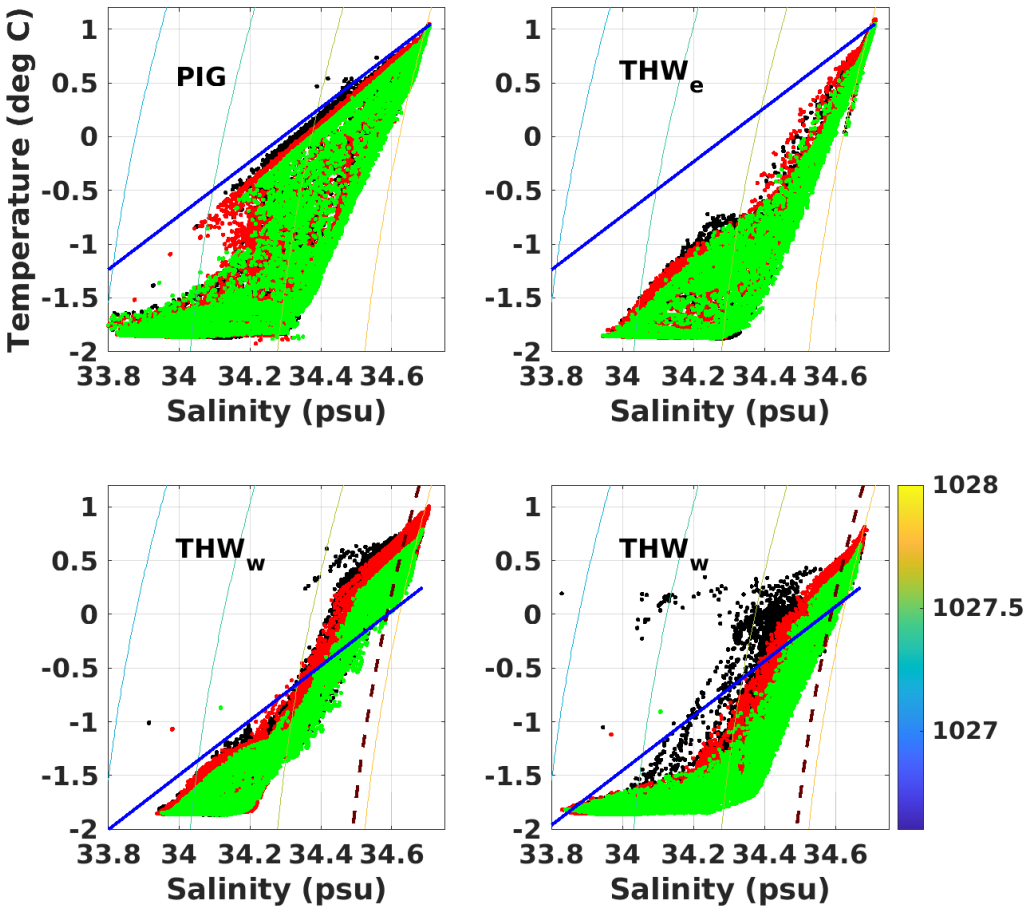

Figure 9. (a) Temperature-salinity diagrams for the **increased** $\mathbf{c}_{fric}$ (red), **runoff** (black), and **baseline** (green) experiments, limited to the Pine Island ice shelf cavity, in June 2011. Isolines of density are shown (parula shading). The solid blue line has the approximate slope of the *Gade* line (Gade, 1979). (b) similar to (a) but under the part of the Thwaites cavity to the *east* of the channel entering the cavity. (c) aimilar to (b) but under the part of the Thwaites cavity to the *west* of the channel. The thick dashed density isoline indicates the density of the ocean cell where runoff is added. (d) Similar to (c) but for June 2013, with black dots indicating output from the **time dependent runoff**, rather than the **runoff**, experiment.

Figure 1.

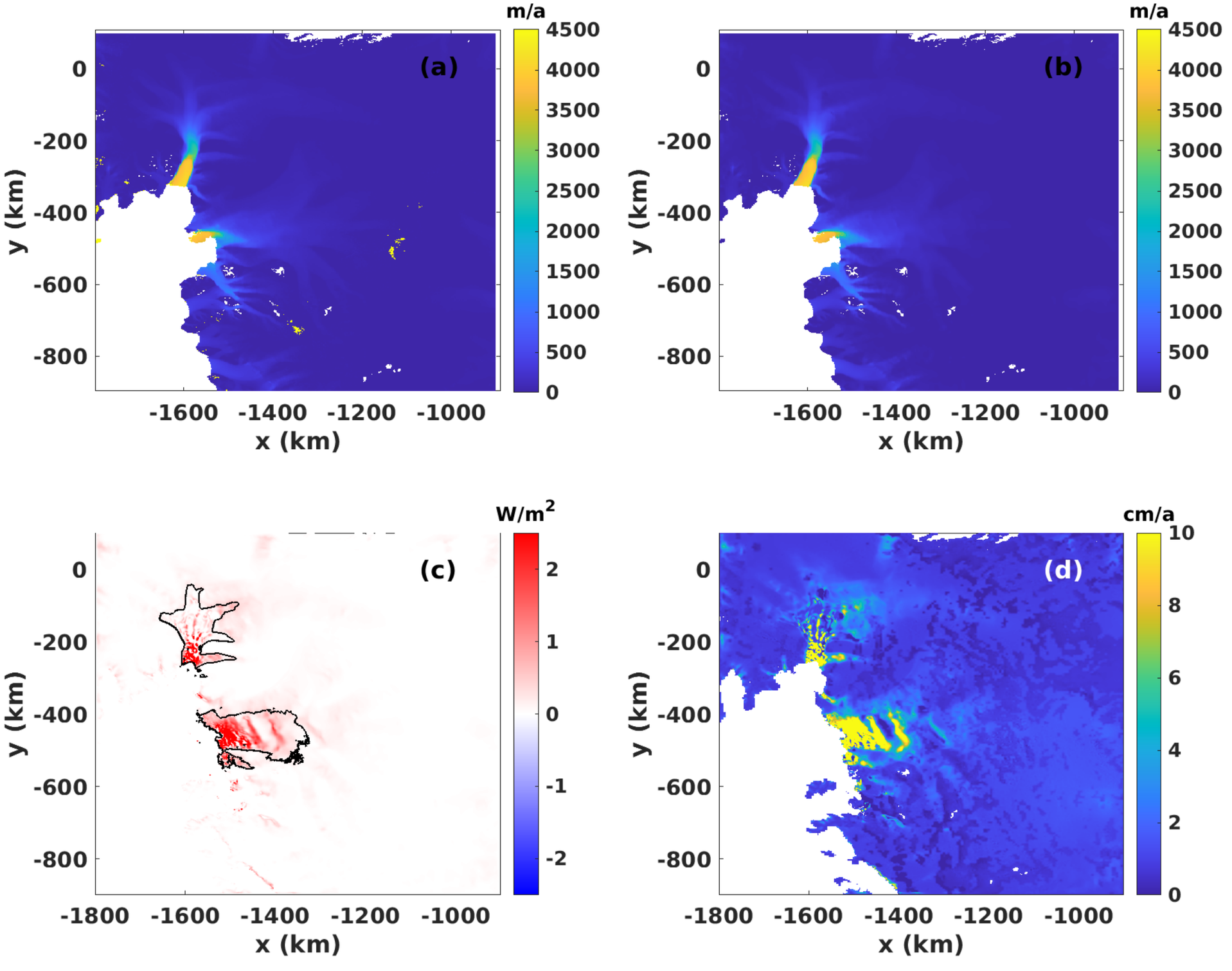
(a)
(b)
(c)
(d)
m/a
W/m^2
cm/a
y (km)
x (km)
0
-200
-400
-600
-800
-1800
-1600
-1400
-1200
-1000
4500
4000
3500
3000
2500
2000
1500
1000
500
0
2
1
0
-1
-2
10
8
6
4
2
0

Figure 2.

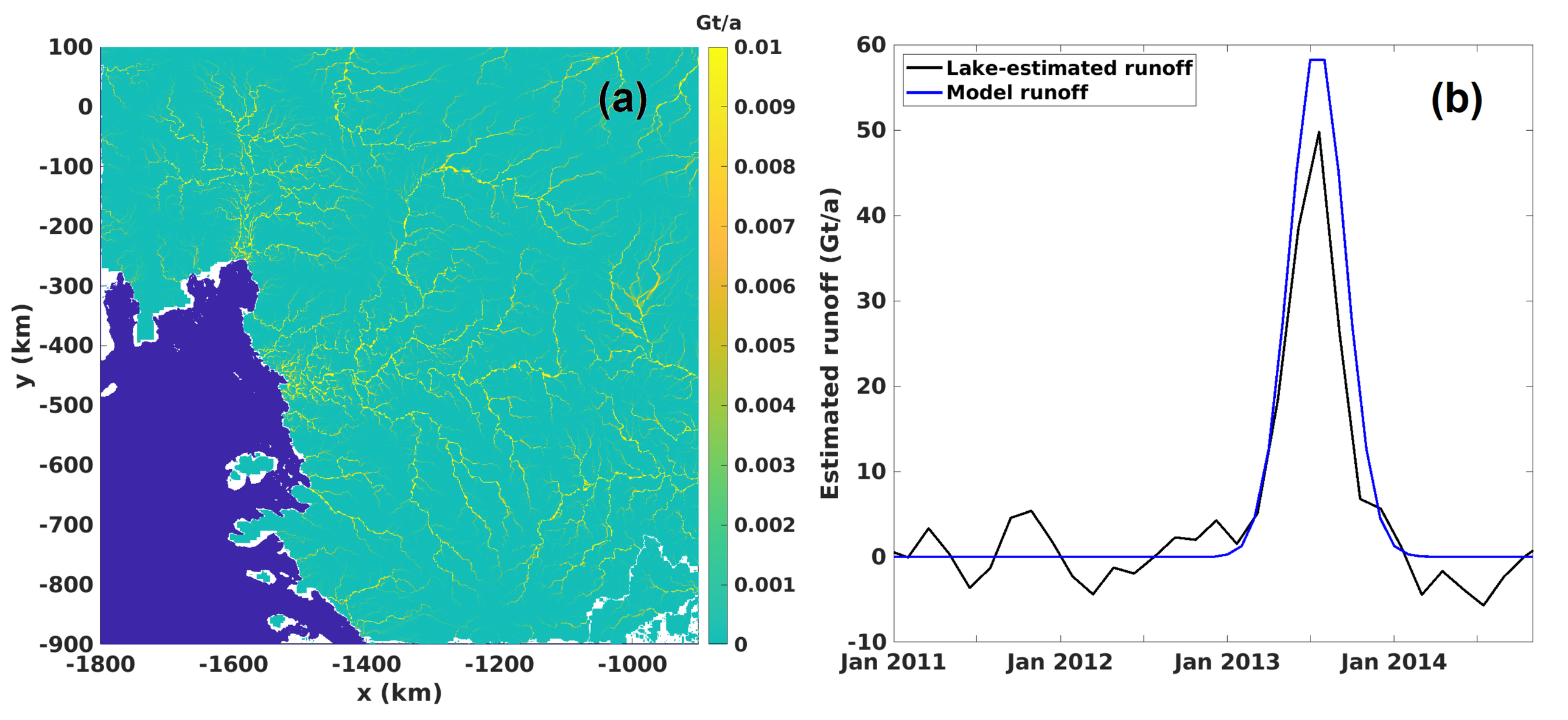
(a)
Gt/a
0.01
0.009
0.008
0.007
0.006
0.005
0.004
0.003
0.002
0.001
0
100
0
-100
-200
-300
-400
-500
-600
-700
-800
-900
y (km)
-1800
-1600
-1400
-1200
-1000
x (km)
(b)
Lake-estimated runoff
Model runoff
Estimated runoff (Gt/a)
60
50
40
30
20
10
0
-10
Jan 2011
Jan 2012
Jan 2013
Jan 2014

Figure 3.

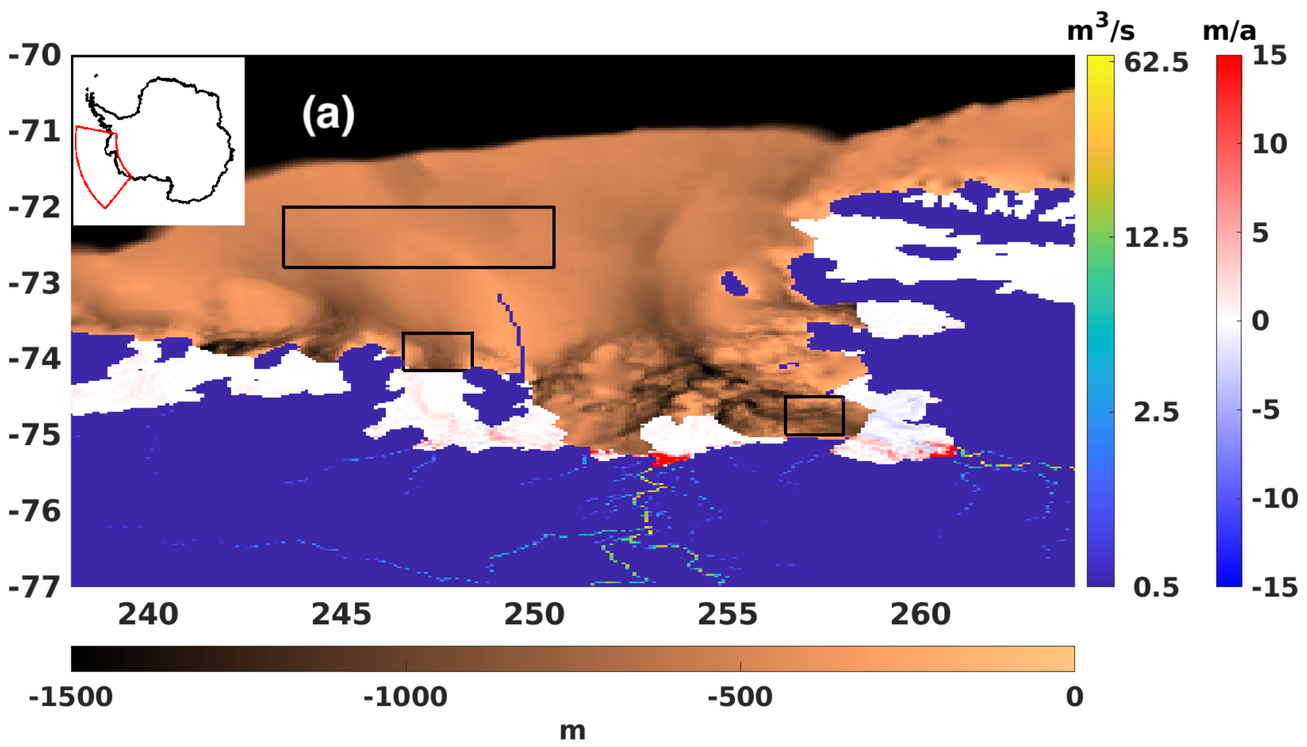
(a)
m³/s
m/a
62.5
12.5
2.5
0.5
15
10
5
0
-5
-10
-15
-70
-71
-72
-73
-74
-75
-76
-77
240
245
250
255
260
-1500
-1000
-500
0
m

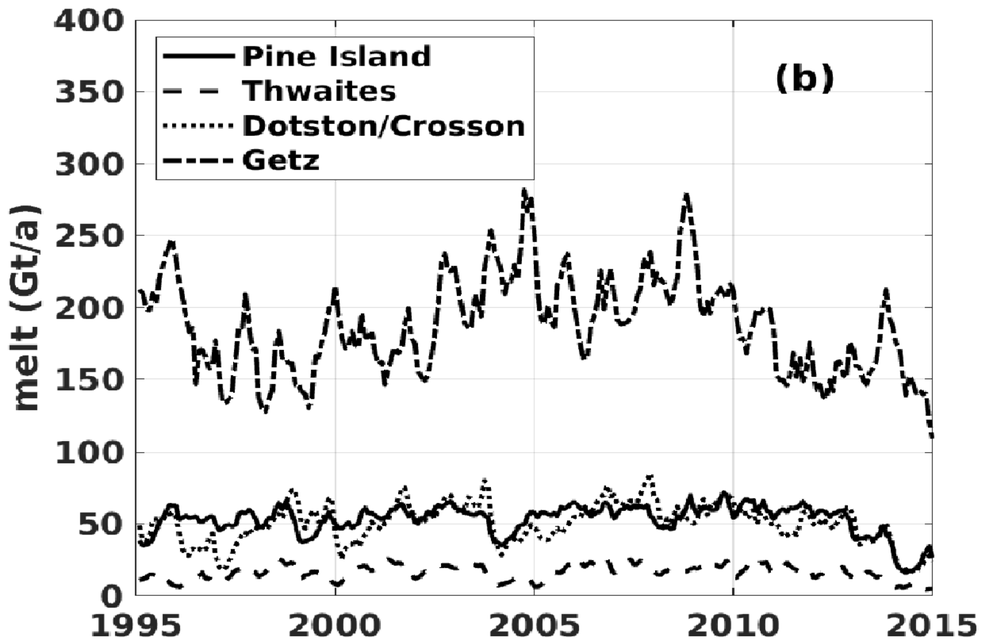
(b)
Pine Island
Thwaites
Dotston/Crosson
Getz
melt (Gt/a)
400
350
300
250
200
150
100
50
0
1995
2000
2005
2010
2015

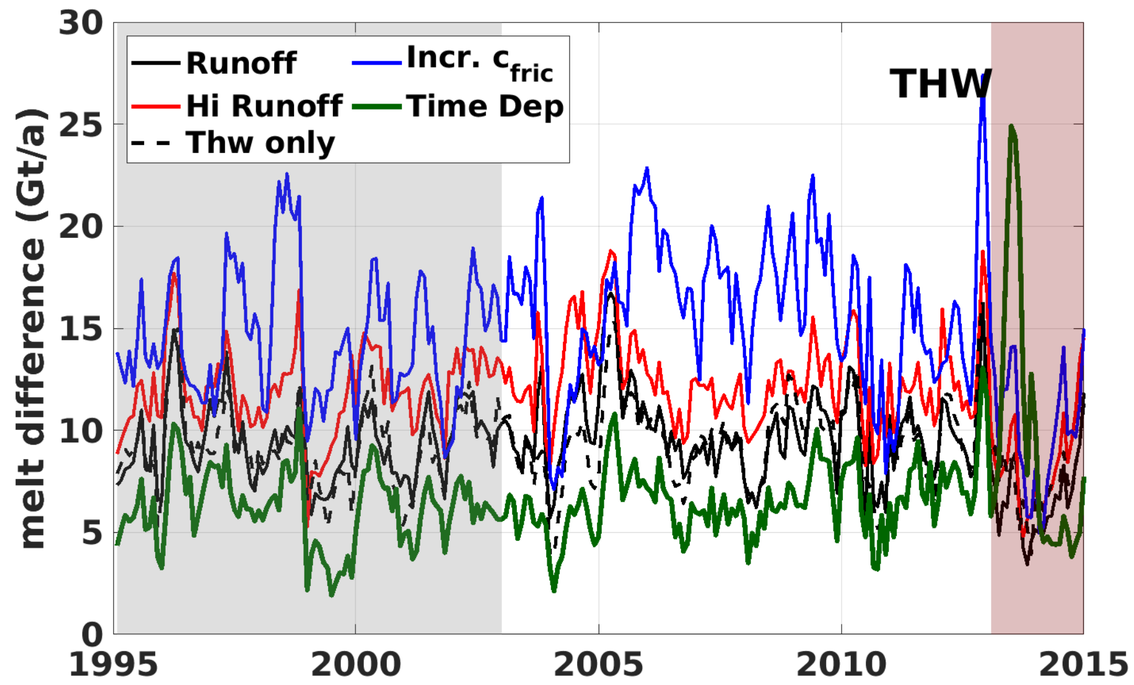
THW
Runoff
Hi Runoff
Thw only
Incr. c_fric
Time Dep
melt difference (Gt/a)
30
25
20
15
10
5
0
1995
2000
2005
2010
2015

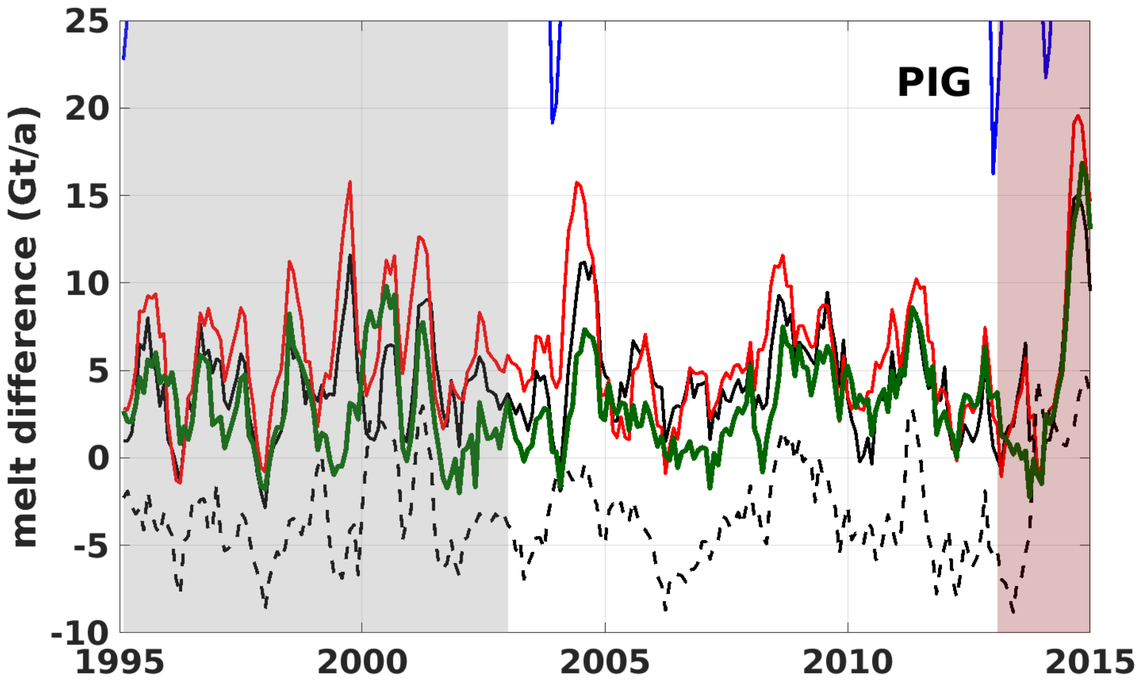
PIG
melt difference (Gt/a)
25
20
15
10
5
0
-5
-10
1995
2000
2005
2010
2015

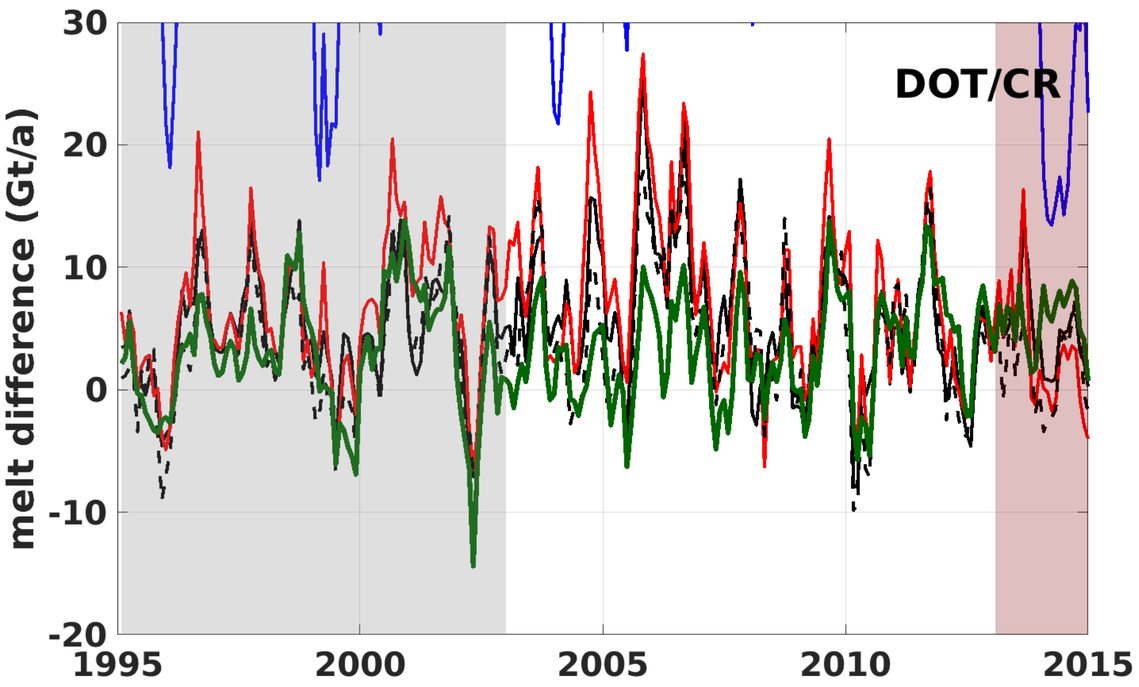
DOT/CR
melt difference (Gt/a)
30
20
10
0
-10
-20
1995
2000
2005
2010
2015

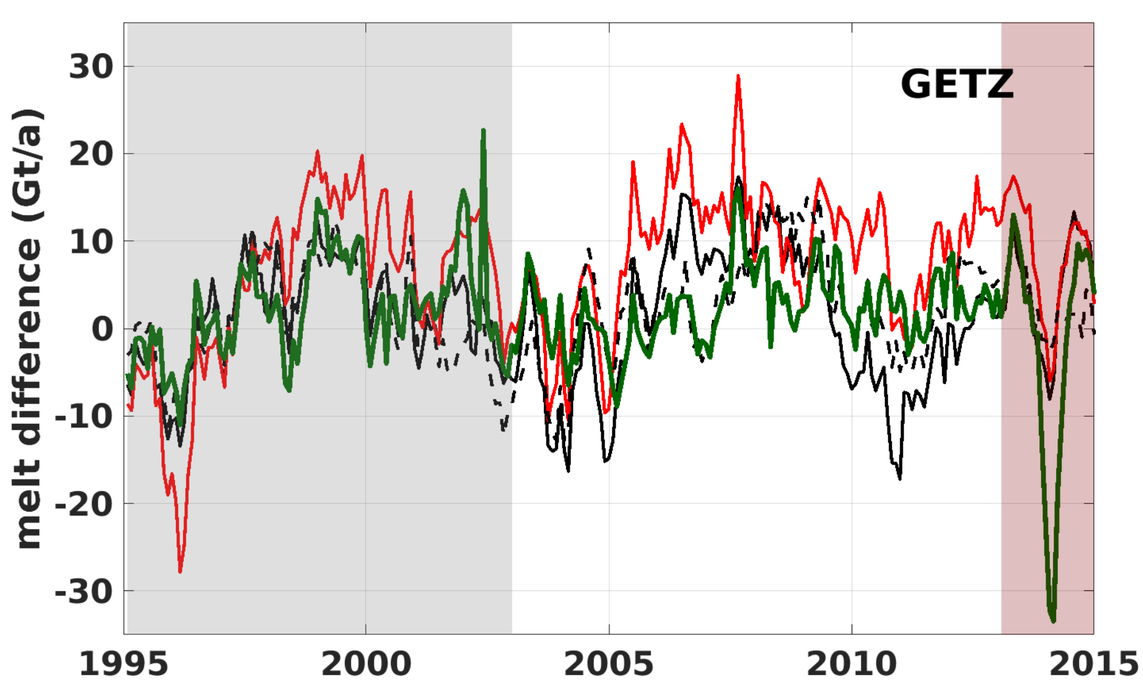
GETZ
melt difference (Gt/a)
30
20
10
0
-10
-20
-30
1995
2000
2005
2010
2015

Figure 4.

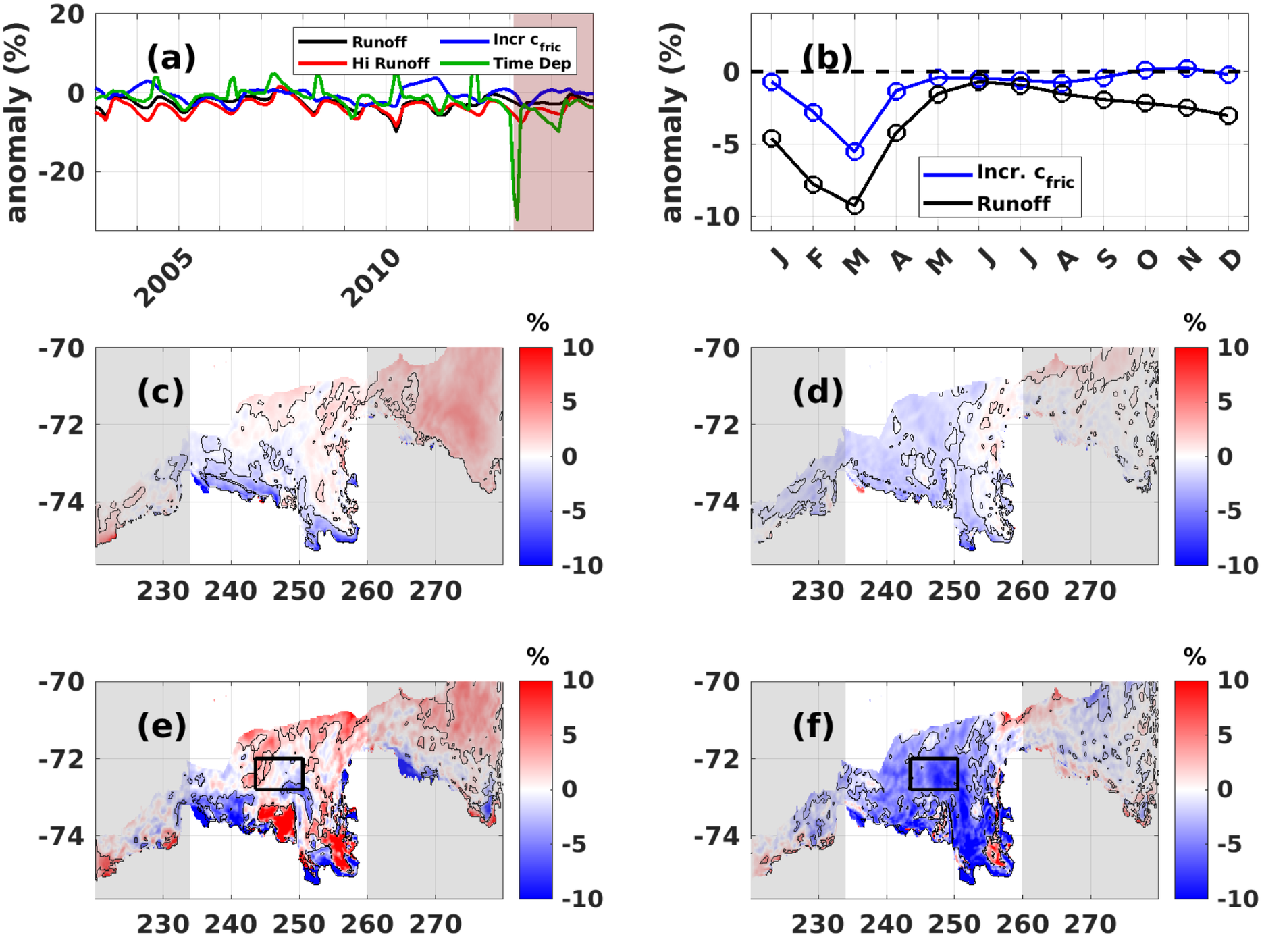
(a)
anomaly (%)
20
0
-20
Runoff
Hi Runoff
Incr c_fric
Time Dep
2005
2010
(b)
anomaly (%)
0
-5
-10
Incr. c_fric
Runoff
J F M A M J J A S O N D
(c)
(d)
(e)
(f)
-70
-72
-74
230 240 250 260 270
%
10
5
0
-5
-10

Figure 5.

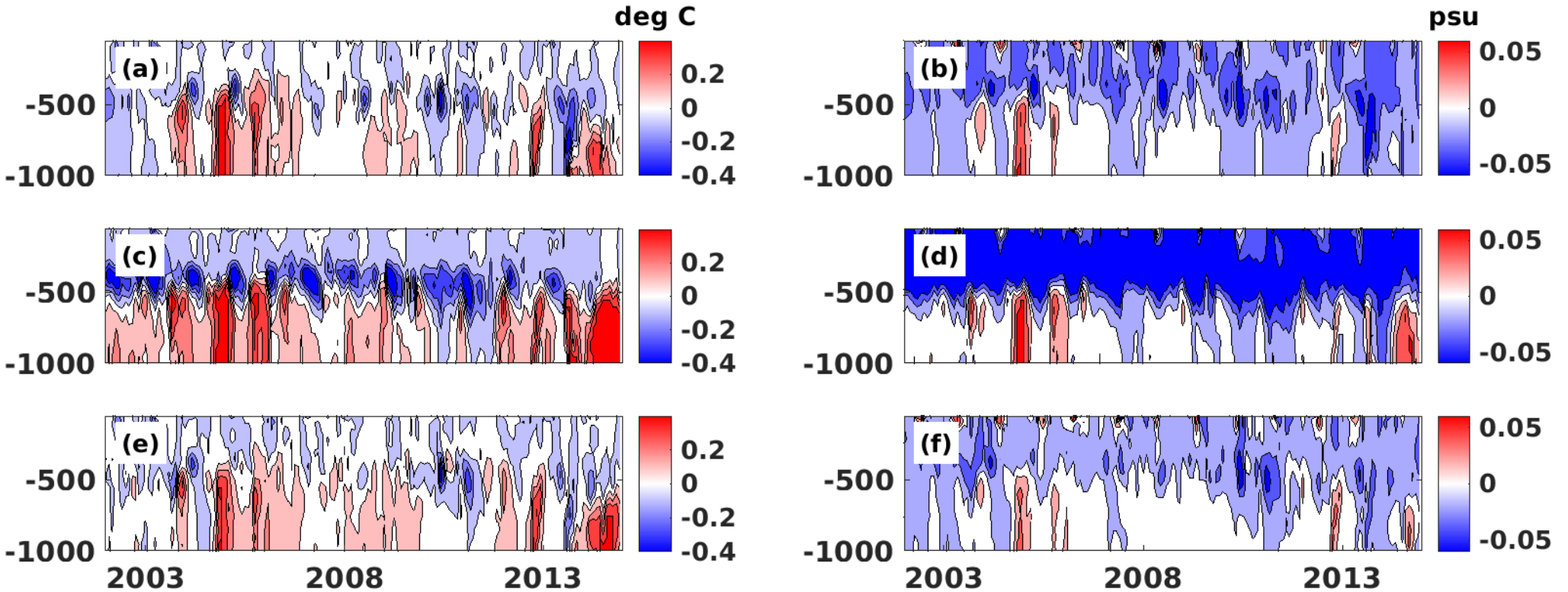
deg C
psu
(a)
(b)
(c)
(d)
(e)
(f)
-500
-1000
0.2
0
-0.2
-0.4
0.05
0
-0.05
2003
2008
2013

Figure 6.

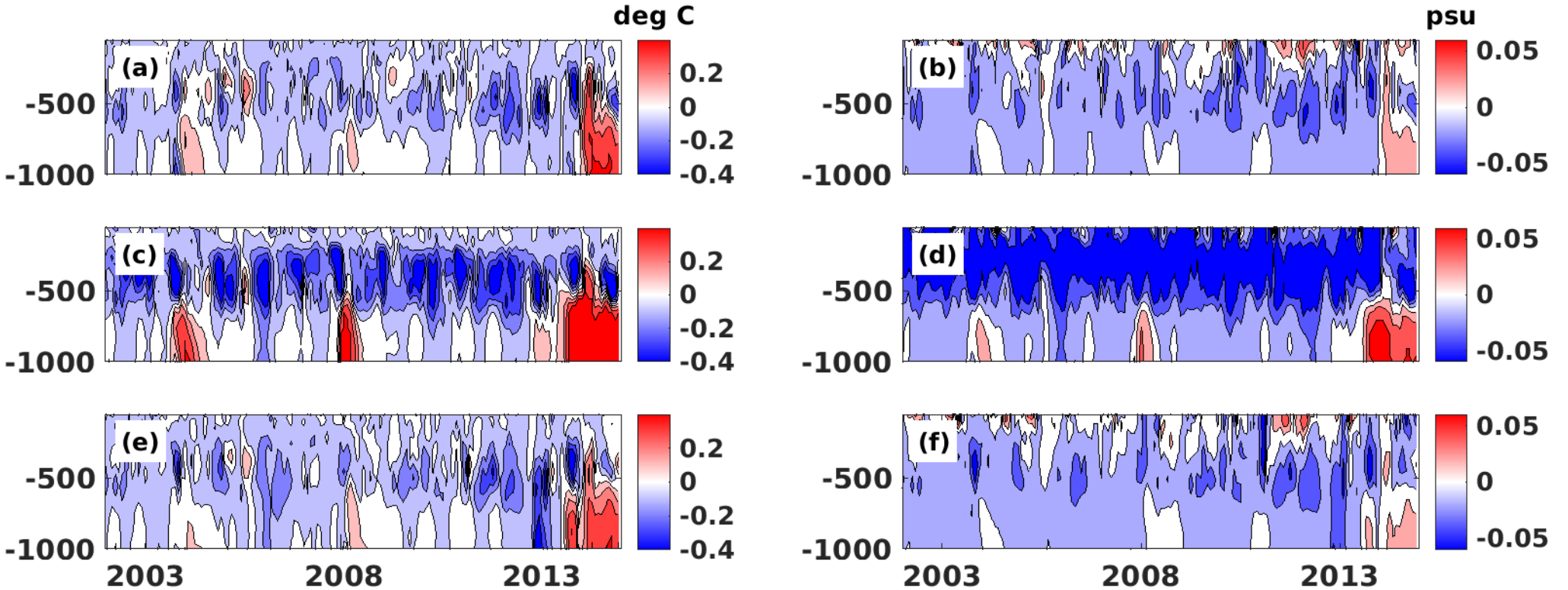
deg C
psu
(a)
(b)
(c)
(d)
(e)
(f)
-500
-1000
0.2
0
-0.2
-0.4
0.05
0
-0.05
2003
2008
2013

Figure 7.

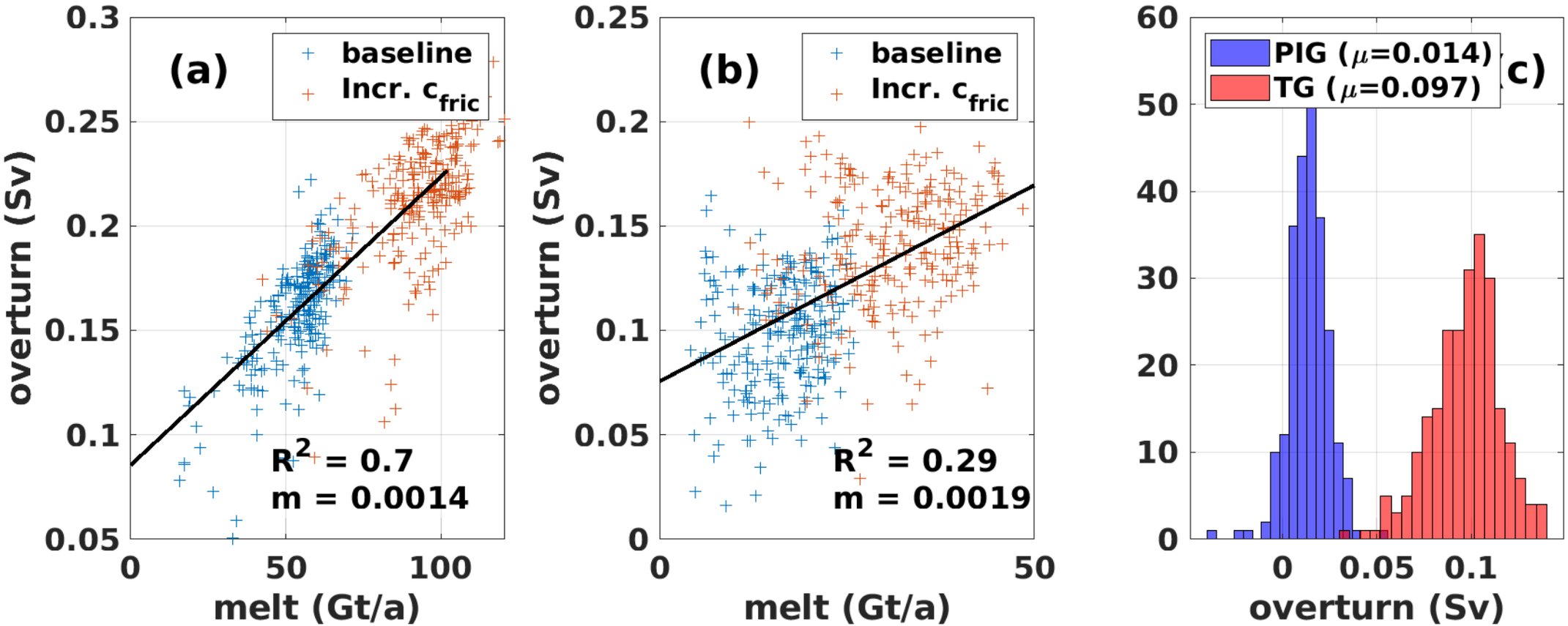
(a)
baseline
Incr. c_fric
R^2 = 0.7
m = 0.0014
overturn (Sv)
melt (Gt/a)
0.3
0.25
0.2
0.15
0.1
0.05
0
50
100
(b)
baseline
Incr. c_fric
R^2 = 0.29
m = 0.0019
overturn (Sv)
melt (Gt/a)
0.25
0.2
0.15
0.1
0.05
0
50
(c)
PIG (μ=0.014)
TG (μ=0.097)
overturn (Sv)
60
50
40
30
20
10
0
0.05
0.1

Figure 8.

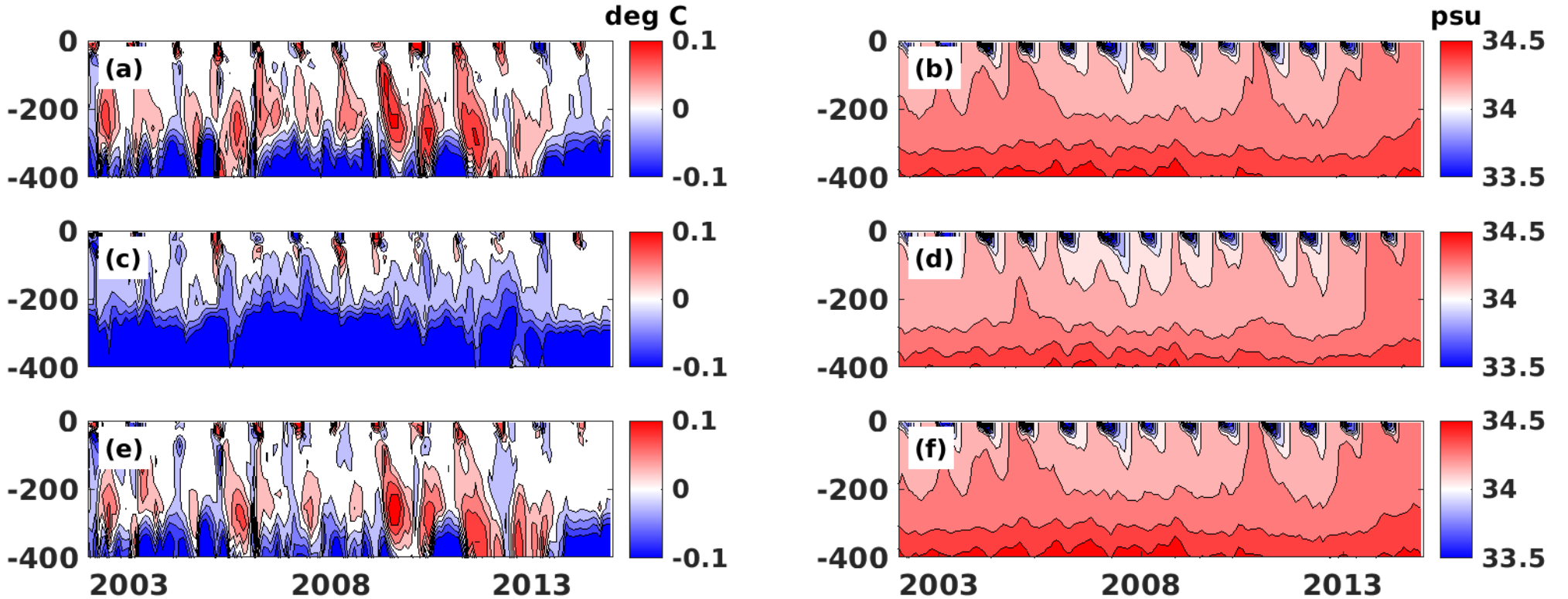
deg C
psu
(a)
(b)
(c)
(d)
(e)
(f)
0
-200
-400
0.1
0
-0.1
34.5
34
33.5
2003
2008
2013

Figure 9.

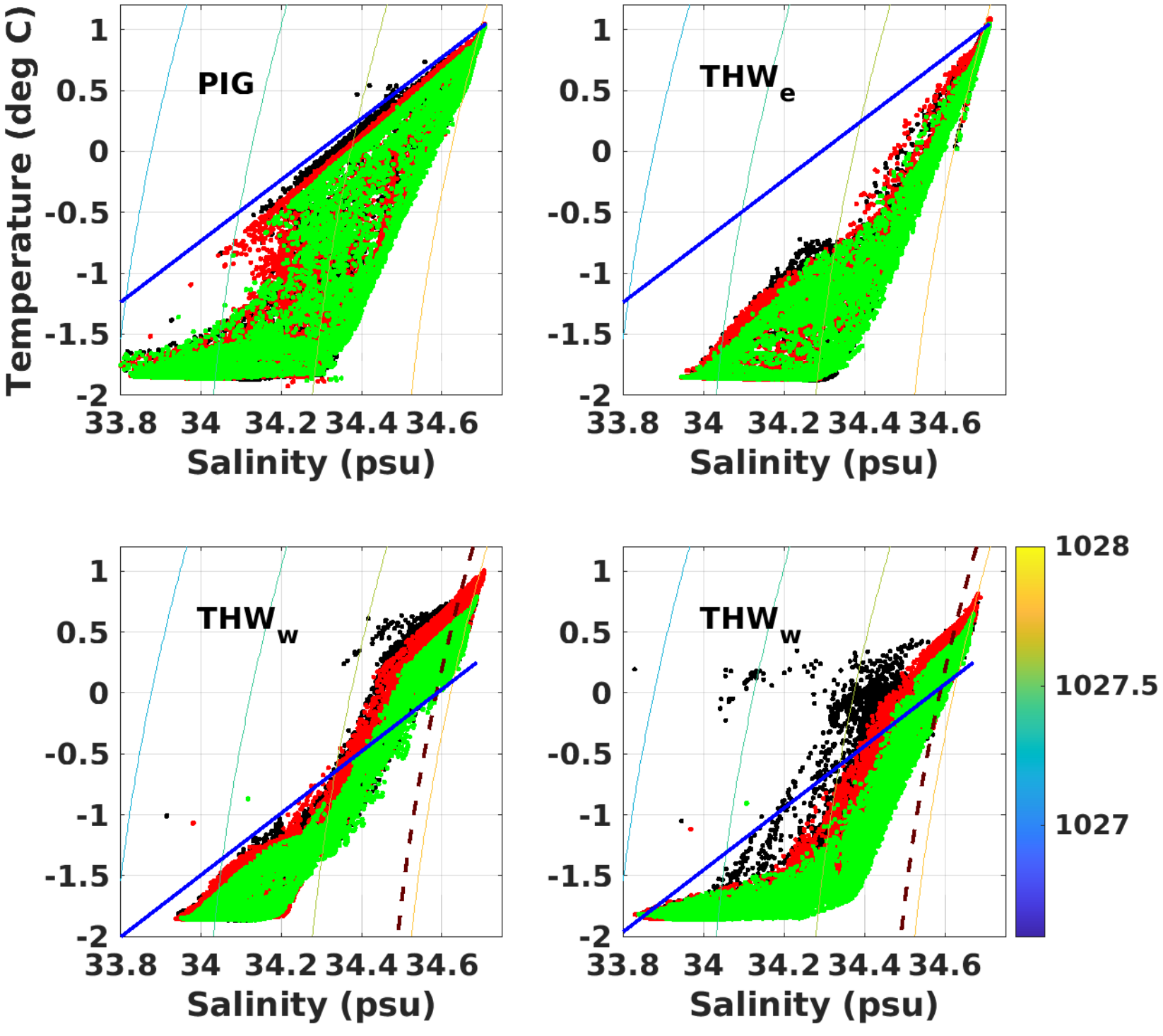
PIG
THW e
THW w
THW w
Temperature (deg C)
Salinity (psu)
Salinity (psu)
Salinity (psu)
Salinity (psu)
1
0.5
0
-0.5
-1
-1.5
-2
33.8
34
34.2
34.4
34.6
1028
1027.5
1027

Supporting Information for The nonlocal impacts of Antarctic subglacial runoff

Daniel N Goldberg[1], Andrew Twelves[1], Paul R Holland[2], Martin Wearing[1]

[1]School of GeoSciences, University of Edinburgh, Edinburgh, UK

[2]British Antarctic Survey, Cambridge, United Kingdom

Contents

March 10, 2023, 6:37pm

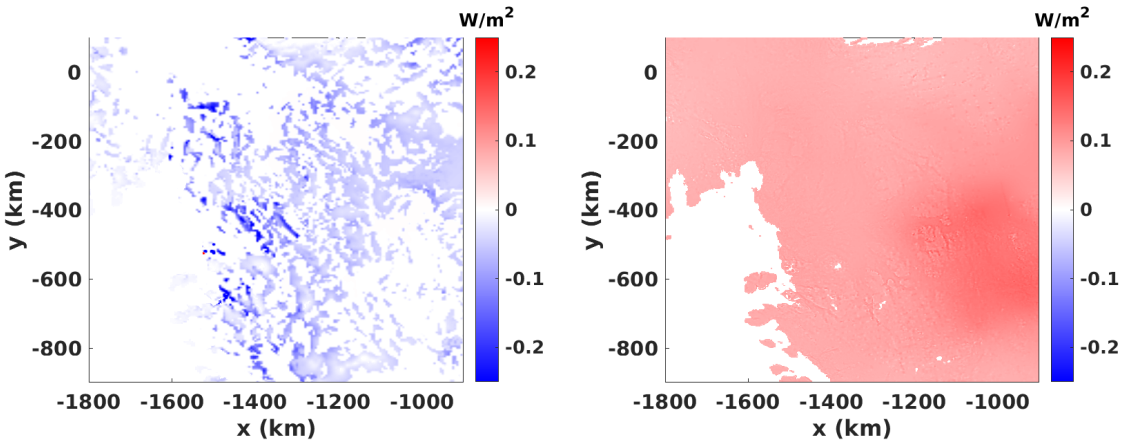

Figure S1. (left) Conductive heat flux associated with vertical gradient of temperature under Amundsen domain used to calculate steady melt. (right) Geothermal heat flux used to calculate steady melt.

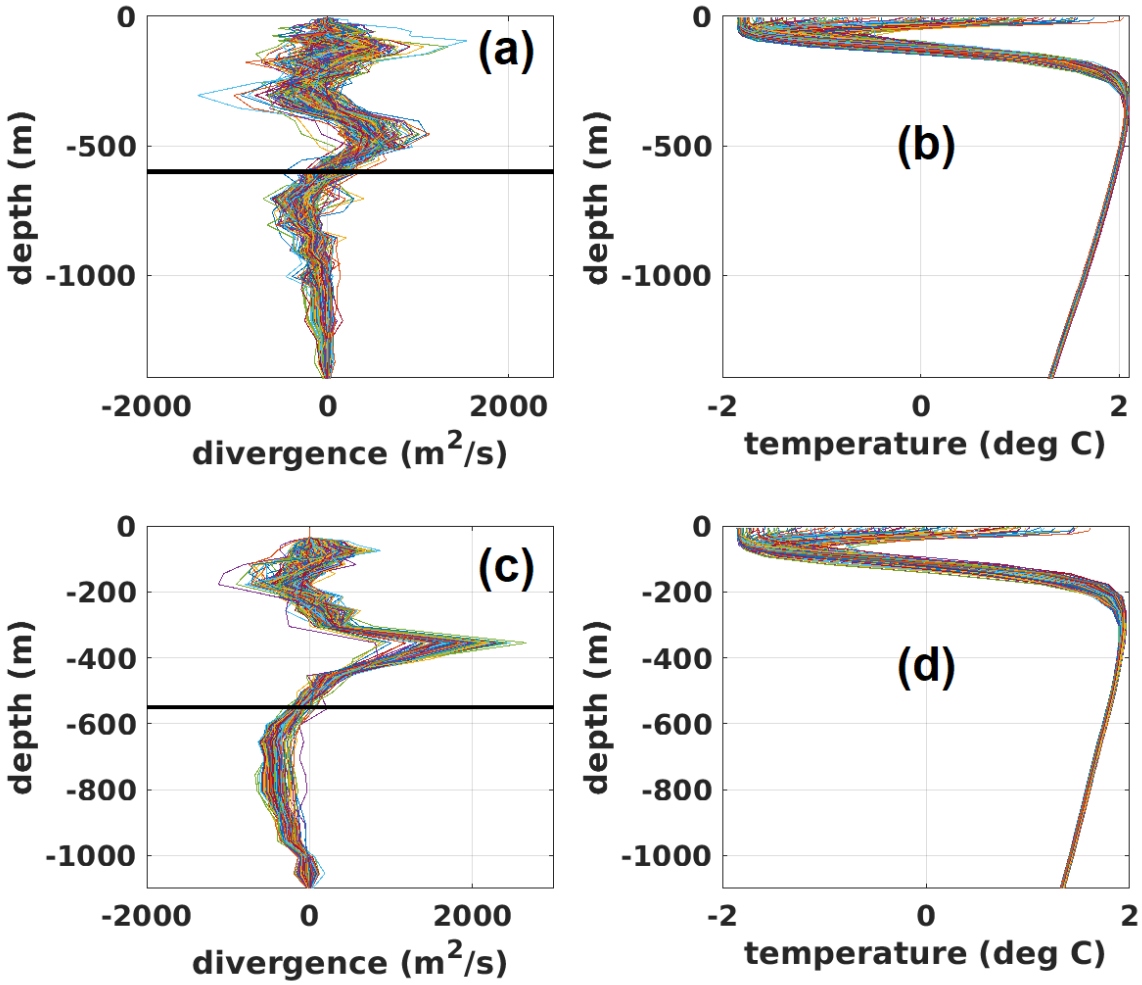

Figure S2. (a) Vertical profiles of horizontal divergence, integrated horizontally over the Pine Island ice shelf cavity. Overturning is diagnosed from a vertical integration below the solid black line. (b) Corresponding mean temperature profiles under Pine Island, indicating that overturning is calculated within the CDW layer. (c), (d): similar to (a),(b) for Thwaites.

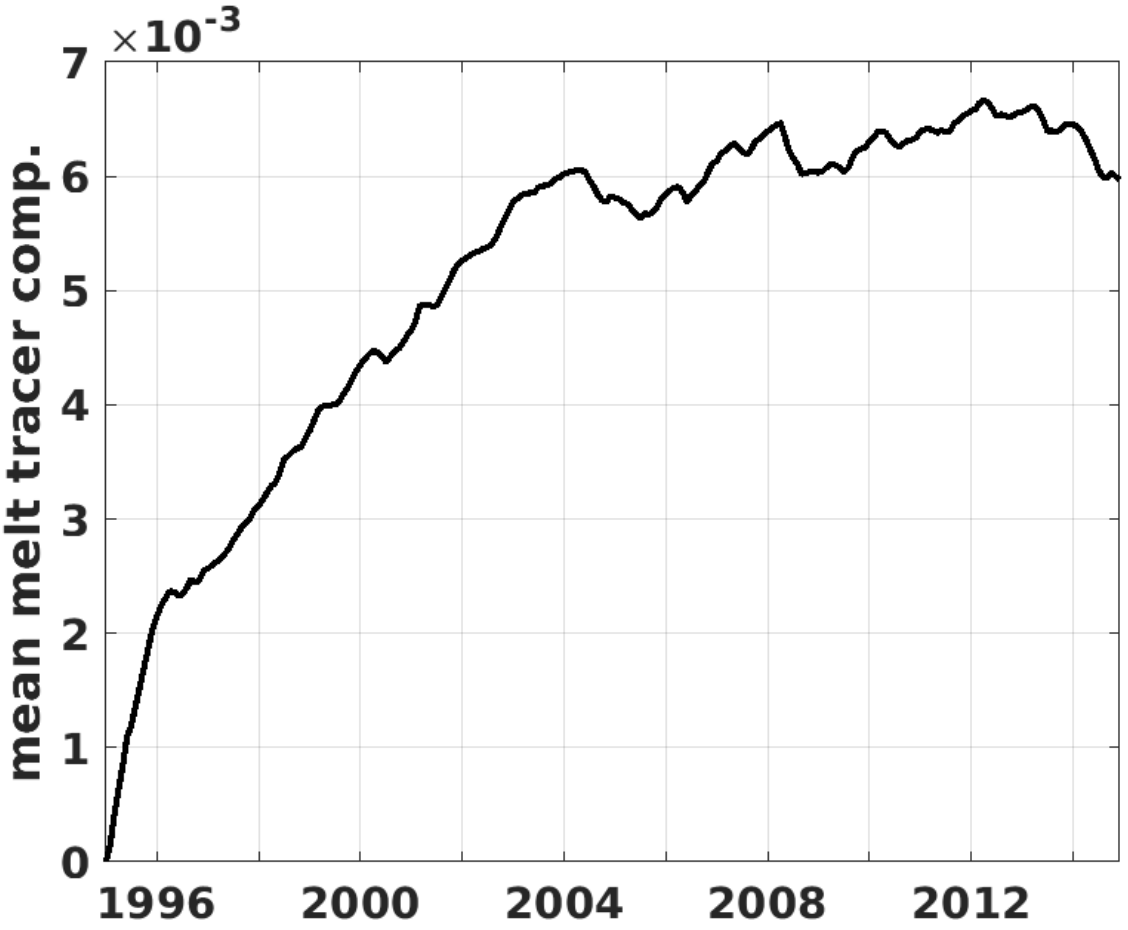

Figure S3. Monthly volume-mean concentration of meltwater tracer in the **baseline** experiment, averaged over the continental shelf.

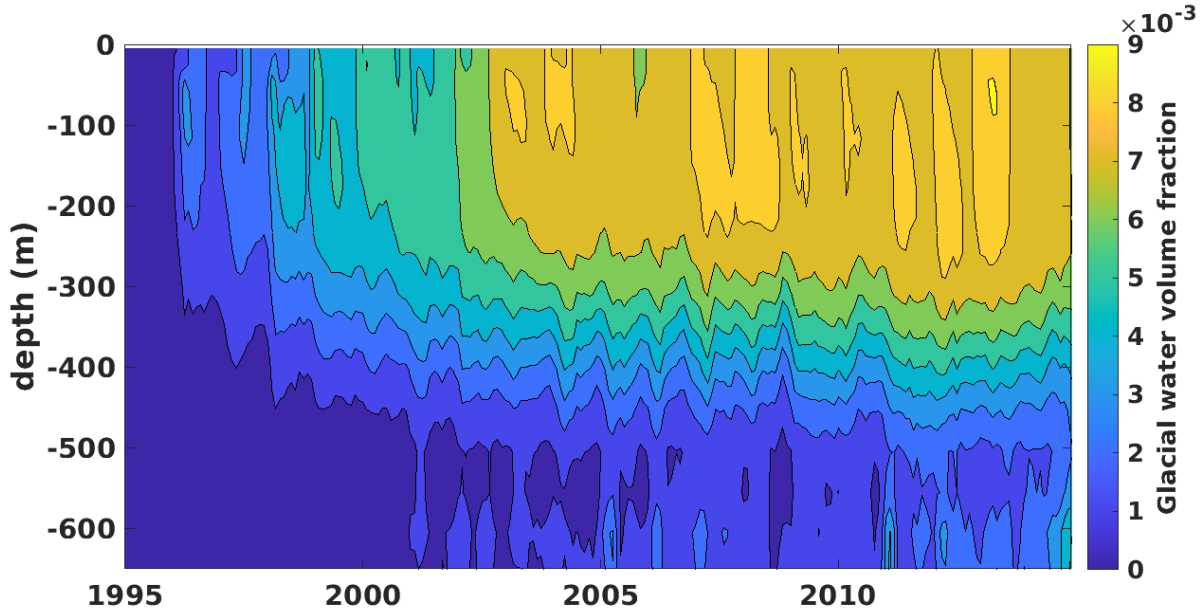

Figure S4. Hovmöller diagram of the volume fraction of the freshwater tracer released from ice-shelf melt, averaged over the region of the continental shelf indicated in Fig 1(a) in the **baseline** experiment. Note this tracer does not include runoff content.

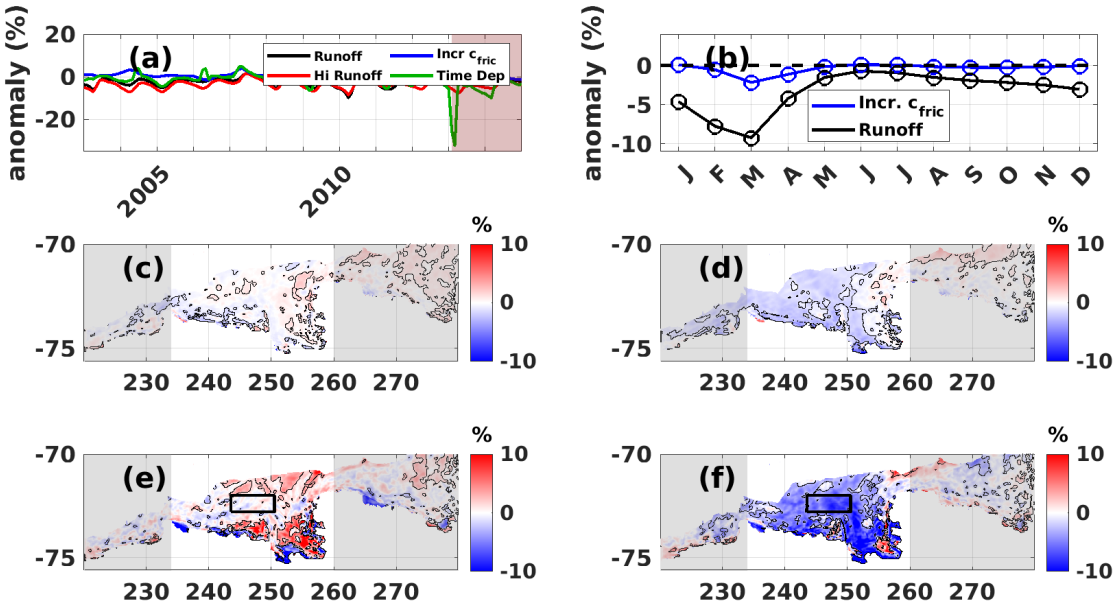

Figure S5. An alternate version of Fig. 4 from the main text, where the mean combined fresh water anomaly from Thwaites and Pine Island in **increased** $\mathbf{c}_{fric}$ is equivalent to that in the **runoff** experiment.